Experimental analysis of an inverted energy harvesting eel

Author

Muhammad Umair

Regn Number

00000203428

Supervisor

Dr. EMAD UDDIN

DEPARTMENT OF DESIGN AND MANUFACTURING ENGINEERING

SCHOOL OF MECHANICAL & MANUFACTURING ENGINEERING

NATIONAL UNIVERSITY OF SCIENCES AND TECHNOLOGY

ISLAMABAD

NOVEMBER 2019

Experimental analysis of an inverted energy harvesting eel

Author

MUHAMMAD UMAIR

Regn Number

00000203428

A thesis submitted in partial fulfillment of the requirements for the degree of

MS Design and Manufacturing Engineering

Thesis Supervisor:

Dr. EMAD UDDIN

Thesis Supervisor's Signature: _____

DEPARTMENT OF DESIGN AND MANUFACTURING ENGINEERING

SCHOOL OF MECHANICAL & MANUFACTURING ENGINEERING

NATIONAL UNIVERSITY OF SCIENCES AND TECHNOLOGY,

ISLAMABAD

NOVEMBER, 2019

THESIS ACCEPTANCE CERTIFICATE

Certified that final copy of MS thesis written by Mr. Muhammad Umair Registration No. 2017-MS-DME-00000203428 of **SMME** has been vetted by undersigned, found complete in all aspects as per NUST Statutes/Regulations, is free of plagiarism, errors, and mistakes and is accepted as partial fulfillment for award of MS/MPhil degree. It is further certified that necessary amendments as pointed out by GEC members of the scholar have also been incorporated in the said thesis.

Signature with stamp: _____

Name of Supervisor: _____

Date: _____

Signature of HoD with stamp: _____

Date: _____

Countersign by

Signature (Dean/Principal): _____

Date: _____

FORM TH-4

MASTER THESIS WORK

We hereby recommend that the dissertation prepared under our supervision by: Student Name Muhammad Umair & Regn No. 203428 Titled: Experimental analysis of inverted energy harvesting eel be accepted in partial fulfillment of the requirements for the award of MS Design and Manufacturing Engineering degree and awarded grade____._____(Initial).

Examination Committee Members

1. Name: Dr. Zaib Ali Signature: _____

2. Name: Dr. Ali Zaidi Signature: _____

3. Name: Dr. Jawad Aslam Signature: _____

Supervisor's name: Dr. Emad Uddin Signature: _____

Date: November 27, 2019

_____ _____

Head of Department Date

COUNTERSINGED

Date: _____ _____

Dean/Principal

Plagiarism Certificate (Turnitin Report)

This thesis has been checked for Plagiarism. Turnitin report endorsed by Supervisor is attached.

Signature of Student

Muhammad Umair

Registration Number

00000203428

Signature of Supervisor

Declaration

I certify that this research work titled "*Experimental analysis of an inverted energy harvesting eel"* is my own work. The work has not been presented elsewhere for assessment. The material that has been used from other sources it has been properly acknowledged/referred.

Signature of Student

Muhammad Umair

2017-NUST-Ms-DME-203428

Language Correctness Certificate

This thesis has been read by an English expert and is free of typing, syntax, semantic, grammatical and spelling mistakes. The thesis is also according to the format given by the university.

Signature of Student

Muhammad Umair

Registration Number

MS-DME-00000203428

Signature of Supervisor

Copyright Statement

Acknowledgements

I am thankful to my Creator Allah Subhana-Watala to have guided me throughout this work at every step and for every new thought which He set-up in my mind to improve it. Indeed, I could have done nothing without His priceless help and guidance. Whosoever helped me throughout the course of my thesis, whether my parents or any other individual was His will, so indeed none be worthy of praise but Him.

I am profusely thankful to my beloved parents who raised me when I was not capable of walking and continued to support me throughout every department of my life.

I would also like to express special thanks to my supervisor Dr. EMAD UDDIN for his help throughout my thesis and for the FEM course which he has taught me. I can safely say that I haven't learned any other engineering subject in such depth than the ones which he has taught.

I would also like to pay special thanks to friends for their tremendous support and cooperation. Each time I got stuck in something, they came up with the solution. Without their help, I wouldn't have been able to complete my thesis. I appreciate their patience and guidance throughout the whole thesis.

Finally, I would like to express my gratitude to all the individuals who have rendered valuable assistance to my study.

Dedicated to my exceptional parents and adored siblings whose tremendous support and cooperation led me to this wonderful accomplishment.

Abstract

Energy harvesting considered to be the ultimate source for long term power supply. Extracting energy from vibration produced in a piezoelectric film gain most attention over a period due to its ability to directly converting mechanical strain energy into electrical energy. In this study, we experimentally investigated energy harvesting from a piezoelectric flag in inverted (whose trailing edge was clamped, and leading-edge was free to move) configuration. Experiment is conducted in open water tunnel under an influence of upstream bluff body to find the impact of energy spectral density of flexible flapping on downstream inverted flag by changing flexural rigidity γ, streamwise gap G_x and Reynolds no. and it's impact on the peak to peak amplitude and voltage generated by piezoelectric flag in term of root means square V_{rms} as well. Vortex induce vibration to occur at downstream of a bluff body in a flowing fluid. Reynolds no. played an important role in our case it's ranges from $10^3 - 10^4$ with vortex street fully turbulent and outside of boundary layer flow remains in a laminar region. It has been observed that as the bending rigidity increases flapping frequency and peak to peak amplitude A/L of a flag decreases results in a decrease voltage generation. Flapping frequency has been measured at different flexural rigidity which shows the variation in energy spectral density. It has been observed that the highest energy spectral density of flexible flapping occurs at flexural rigidity of $0.01\ \mathrm{N.m^2}$. Image processing technique is used to find out peak to peak amplitude and using Fast Fourier Transform (FFT) to find out a dominant flapping frequency in a MATLAB. Output voltage from a piezoelectric flag is being measured using a DAQ (a module in a LabView for accruing analog output voltage). Particle Image Velocimetry used to find vortex interaction with the inverted flag at downstream of the bluff body and a Strouhal number from particle movement in successive frame.

Key Words: *Inverted flag, Vortex Induce Vibration (VIV), Piezoelectric, Particle Image Velocimetry (PIV), Spectral density*

Table of Contents

List of Figures

List of Tables

CHAPTER 1: INTRODUCTION

Due to the limited resources of fossil fuels, the increase in demand and their environmental impacts, the search for harvesting energy from renewable resources is increased. In recent years, most of the research has been done on the flapping dynamics of flexible structures in a fluid flow and energy harvesting through it. Piezoelectric patches attached to the flexible structures can convert the strain energy caused by its deformation into electrical energy. The deformation can be from different sources, such as human motion, acoustic noise, fluttering flag, flapping birds, etc. This is a kind of renewable energy resource. In nature, especially the aquatic animals like the motion of fish in water behaves like a flexible structure in fluid flow affects the motion of other fish behind it because of their vorticity effect. To mimic this phenomenon, a thin flexible sheet in any fluid flow like water or air can cause the deformations in the sheet. These deformations can be used to generate electric current. A thin sheet is termed as a flexible flag.

1.1 Background, Scope and Motivation

Fluid-structure interaction (FSI) is an interaction between a deformable structure and a fluid flowing around it. It is a prime consideration in designing many engineering systems. Energy harvesting considering the effect of fluid-structure interaction from the ambient environment is an effective approach to sustainable green power (solar, wind and ocean waves). Much of the research work has done either experimentally or numerically to find a way of harvesting energy from an interaction of a flag made up of different materials like PVDF piezoelectric membrane, polycarbonate, etc.

The flexible flag can have two configurations. One having clamped leading edge and free trailing edge, termed as a conventional flag, while the other having a free leading edge and clamped trailing edge is termed an inverted flag. Both can flap in a uniform flow or behind the bluff body. There are two energy conversion processes in this phenomenon. First the kinetic energy of the fluid flow is converted into the strain energy of the flag, second, this strain energy stored in the flag is converted into electrical energy through piezoelectric patches attached on its surface[1]. Recent work has been started on the novel arrangement of an inverted flag[2]–[4].

CHAPTER 2: LITERATURE REVIEW

Different configurations with conventional and inverted flags were used by many researchers to induce large oscillations and flapping amplitudes like tandem, side by side and multiple flags in diamond or X-shaped arrangement. Downstream bodies are strongly influenced by the vortices shed by an upstream body. Vorticity interaction with a downstream flexible flag in tandem arrangement using conventional configuration was examined including the bending coefficient, frequency, phase angle and flapping amplitude of pitching and heaving motion. It was observed that the drag coefficient of the downstream flag was only slightly dependent on the gap distance between the two flags [5].

2.1 Conventional Flag

A flag whose trailing edge was free to move while the leading edge was fixed, termed as conventional flag configuration. The fluid flows after passing on bluff body a case of vortex-induced vibration (VIV) or in a case without a bluff body termed as flow-induced vibration (FIV) approaches the trailing end of flag causes it to flap. Conventional flag exhibits three modes, a straight stretched mode, fluttering mode, and periodic flutter mode. Peak to peak amplitude (A/L) of a conventional flag is 0.8.

Cantilever elastic sheet suspended in a uniform flow undergoes self-sustained oscillation due to fluid-structure interaction. In past research has focused on a conventional flag where leading edge is fixed and trailing edge is free to move[6]–[10]

The interaction between a conventional flexible flag and uniform flow in triangular, diamond and conical formations was investigated as a function of both bending coefficients and the gap distance between the flag [11]. Coupling performance of two identical flags in side-by-side, parallel, tandem and staggered positions was studied in detail. Significant drag reductions were observed in the in-phase flapping mode for relatively small separation in parallel position [12].

2.2 Inverted Flag

On the other hand, a flag whose trailing end was fixed, and leading-edge could flap freely termed as the inverted flag. The concept of inverted flag was mimicked by flapping leaves due to

the air passing through it [13] and dynamics of hair is also one of its example This is the fact that a mechanical model with free front end and clamped rear end is generally more unstable to external axial loading than a clamped front end and a free rear end.

Daegyoum Kim experimentally investigated the dynamics of an inverted flag and condition of self-excited flapping. Flapping sheets can produce strain energy several times larger than deformed mode thus improving the conversion of fluid kinetic energy to mechanical strain energy. The results show that an inverted flag displays a large peak to peak amplitude up to 1.7-1.8 than a typical flag since the aerodynamic force either is lift and drag tend to destabilize flag hence produce a deformation. Flapping occur within a narrow range of non-dimensional bending stiffness so as the periodic conversion of strain energy and moreover its instability is independent of mass ratios[2].

Jaeha Ryu numerically investigated the flapping motion of an inverted flag in a uniform flow considering the immersed boundary method. He examined the vortical structures and flapping dynamics of inverted flag in a uniform flow in terms of bending rigidity (γ) and the Reynolds number. The maximum mean strain energy was gained when a vortical structure behind an inverted flag formed a vortex pair during a flapping mode. In his findings, it stated that large peak-to-peak amplitude (A/L) and bending rigidity are proportional to mean strain energy. The bending rigidity of an inverted flag is 100 times larger than the conventional flag as a conventional flag at certain bending rigidity does not exhibit a self-sustained flapping. Mean strain energy in a biased mode is 10-20% more than the maximum mean strain. It was concluded that peak-to-peak amplitude influenced the dynamics of inverted flag and its energy harvesting efficiency. As the maximum strain energy was obtained near the trailing edge so, piezoelectric patches to be attached as close as possible near the trailing edge[3].

Orrego experimentally investigated wind energy harvesting of flexible piezoelectric membrane in an inverted configuration. He studied the flapping dynamics of a thin sheet in inverted configuration to observe its stability effected by parameters like bending rigidity, free stream velocity, density and flexible sheet length. It was found that for the instability of inverted flag, mass ratio was not an important factor. In his finding reported that $0.4\mathrm{m\,W/cm^3}$ power

produced at low airspeed of $3.5\,\mathrm{m/s}$. Inverted flag with higher aspects and mass ratio harvested greater electrical energy due to higher bending curvature and faster flapping frequencies[14]. Sader stated that at low flow speed flag maintains its position and remains in straight mode, within a velocity range it starts flapping with large amplitude after that it got deflected on one side and remains in deformed state[15]. Rinaldi and Païdoussis investigated the effect of flow orientation on cantilevered slender cylindrical rod. It has been observed that rod exhibits small flutter at low flow speed. As changing direction dynamics of flag have been changed flag undergoes more deformation than conventional flag due to either drag or lift force exerted on it[16]. Tang discussed in detail about flapping modes, effects of the mass ratio, inclination angle, the Reynolds number (Re), elastic strain energy and vortical structures around the plate[17].

Shoele and Mittal coupled the piezoelectric mechanism with inverted flag in a uniform flow followed by comprehensive study on the effects of bending rigidity, flag inertia and Reynolds number with vortical structures[18]. Kim experimentally investigate the dynamics of two types of downstream flag, a conventional and an inverted flag, on and off a midline behind an upstream bluff body in water and air flows. Maximum flapping amplitude reached by the inverted flag behind the bluff body was almost constant and the flapping behavior in both water and air flow was similar. An inverted flag behind the bluff body showed sharp transition to the large amplitude at certain free-stream velocity of 2.8 when the flag is far from the bluff body at G_x 1.67 and 2.00. Like conventional flag, simulations on inverted flag in a uniform flow were carried out for side by side arrangement to study the flapping dynamics, flag properties in dimensionless parameters and spanwise gap distance between them[19].

2.3 Fundamentals of Vortex-Induced Vibration

Mobasher in 2012 discussed the basic concepts of Vortex-Induced Vibration along with its parameters. The vortices are generated alternatively from one side to the other and in result of these vortices at the back of the object, unsteady oscillating pressures are generated which cause the object to vibrate[20]

2.3.1 Vortex Shedding at different Reynolds No.

No vortices are generated at Reynolds Number equals to or less than 5. Nishioka in 1978 experimentally studied the wake behavior downstream of a cylinder at Reynolds Numbers between

20 to 150. A low-speed wind tunnel was used for this purpose with a range of flow speeds of 10 to 100 cm/s. The very first time the vortices are generated in this Reynolds numbers range and their lengths get increases as the Reynolds number increases. The length of the vortices can reach up to 3 times the diameter of the cylinder at Reynolds Number 45 [21]. Effects on the vortices by increasing Reynolds number beyond 45 has been studied by Huerre and Monkewitz in 1990 and they proposed that the stability of the wake is disturbed[22]. Friehe in 1980 carried an experiment to observe the shedding frequency and velocity of the free stream passing by cylinders of length to diameter ratio of greater than 150. The range of Reynolds number was from 50 to 175. Results show that the breakage of one of the vortices happened in this range[23].

Anatol Roshko in 1954 selected Reynolds number ranges from 40 to 10000 and using wind tunnel, analyzed the wake dynamics behind circular cylinders of diameter ranges from 0.0235 to 0.635 cm. Based on the flow dynamics, two ranges were set. Below Re=150 was a stable range where the flow was laminar and viscous configuration was dominant. Beyond 150, the range was a transitional range where turbulence got involved. Only the vortices in the wake region are turbulent. The boundary layer is still laminar. Roshko in 1961 observed an increase in drag coefficient of over a large cylinder placed in a wind tunnel for experimentation purposes. The range of Reynolds numbers selected was 106 to 107. Results show the drag coefficient increment from its supercritical value and attaining 0.7 at Reynolds number 3.5*106. Also, vortex shedding started to occur again with the complete turbulence of vortices as well as the boundary layer. Nickerson and Dias in 1981 proposed by the help of experimentation that vortex shedding can occur up till Reynolds number 1011.

2.3.2 Vortex Shedding across cylinder

Griffin and Ramberg in 1975 investigated the wake formation downstream of a rigid cylinder. Results of their investigation showed that when the cylinder vibrates with a frequency approximately equal to the frequency of vortices being shed, vortices are shed with a great strength. Bishop and Hassan in 1964 presented findings of their experiment and showed that the cylinder experiences more drag force.

2.3.3 Vortex Shedding across flat plate

Teimourian in 2017 reviewed numerically the vortex shedding downstream of a flat plate having different arrangements consisting of single plate, tandem, and side by side arrangements. Most of the literature has been covered on a single plate. Among the different turbulent models, direct numerical simulation (DNS) is mostly used by researchers. Bently and Mudd investigated the shedding effect and the effects of gap distance for various bluff bodies. He concluded that bluff bodies that are closely spaced in a tandem arrangement have the same behavior as a single body. As the gap is increased, vortices start to separate from the bluff body and the effects of these vortices start to appear.

2.4 Vortex Generation and Shedding

2.4.1 Vortex Generation

As the fluid passes a solid object at low Reynolds Numbers I.e. Re<=5, the fluid follows the shape of the object all away around and passes smoothly. The streamlines of the fluid will have symmetric configuration around the body with oscillating high pressure at the front and back and low pressure at the top and bottom of the object placed inflow stream. As the Reynolds Number passes the barrier of 5, vortices start to form at the back of the object. In the case of the flapping flag, these vortices are formed alternatively from both sides. They remain inside the wake behind the body until a certain number.

2.4.2 Vortex Shedding

Vortices start to break from the object as the Reynolds number approaches almost 100. Flapping of the flag propels the vortices and new vortices take place of the previous ones. In the case of multiple flags in tandem or staggered arrangement, these vortices of the former flag interfere with the vortices of the rear flag constructively or destructively depending upon the streamwise and spanwise gap between the two flags. The increment or decrement of the amplitude and drag force acting on the rear flag depends on whether the vortices are meeting constructively or destructively. Lienhard in 1966 studied the vortex generation and shedding downstream of a cylinder at different Reynolds number represented in figure 4

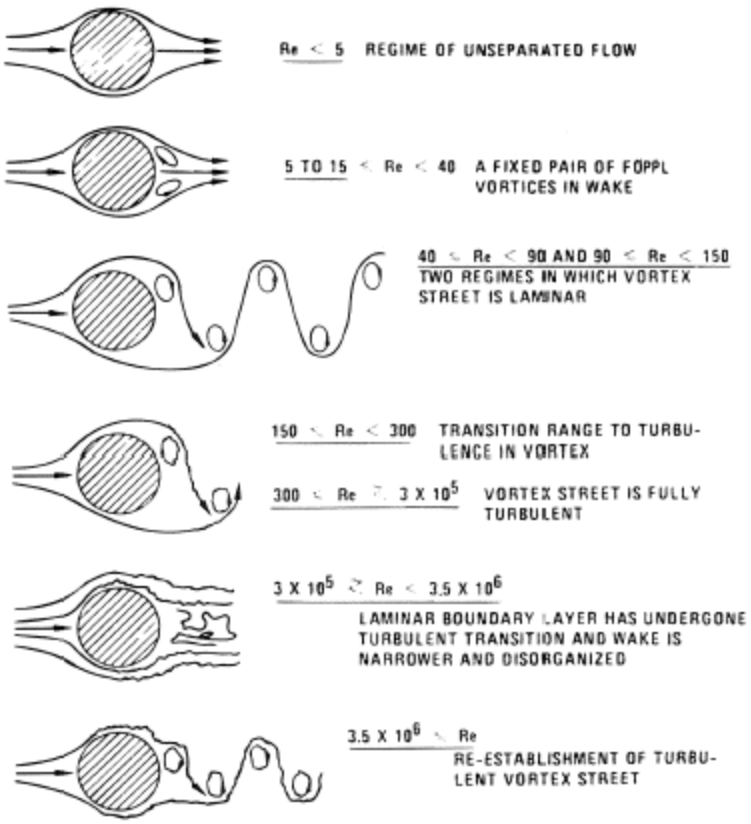

Figure 2-1: Vortex shedding at different Reynolds No. at downstream of circular cylinder[24]

2.5 Blockage Ratio

Choi in 1998 experimentally investigated the blockage ratio of a square model wind tunnel. The cross-section of the test section is 1*1 m with a maximum velocity of 17 m/s. The findings of his research is that the blockage ratio can be allowed up to 10% with negligible effects on the experiments[25].

2.6 Basic Definitions

2.6.1 Viscosity

Viscosity is the internal resistance between the two neighboring layers of flowing fluid.

2.6.2 Kinematic Viscosity

Kinematic viscosity is the dynamic viscosity per density of the fluid.

2.6.3 Blockage Ratio

It is defined as ratio of the area of the model perpendicular to the flow to the cross-section area of the test section. It should not cross 5% for better results.

2.6.4 Angle of attack

Angle between the reference line of the structure and the oncoming fluid is known as angle of attack.

2.6.5 Critical angle of attack

It is the angle of attack at which maximum lift coefficient can be attained. Below this angle, lift coefficient has direct relation with angle of attack. Mostly this angle is around 15 to 20 degree.

2.6.6 Stalling

Reduction in lift coefficient at larger angle of attack when the critical angle of attack is exceeded which is almost 15 degrees due to separation of airflow from the airfoil.

2.7 Basic Formulae

2.7.1 Bending Stiffness

It is defined as the opposition proposed by the structure to the bending deformation.

$$K_b = \frac{Eh^3}{12(1-v^2)\rho_f U^2 L^3}$$

2.7.2 Mass Ratio

Mass ratio in fluid mechanics is the ratio of the mass of the substance to the mass of the fluid containing it.

$$M = \frac{\rho_h}{\rho_f L}$$

2.7.3 Reynolds Number

It is dimensionless number representing the ratio of the inertial force to the viscous force inside the fluid. Reynolds number differentiate between the laminar and turbulent flow.

$$Re = \frac{\rho UL}{\mu}$$

2.7.4 Froude Number

A dimensionless number defined as ratio of flow inertial force to the external or in specific gravitational force is known as Froude number.

$$F_r = \frac{U}{gl^{1/2}}$$

2.7.5 Strouhal Number

A non-dimensional number which is used to analyze the dynamics of unsteady fluid flow. It represents the relation between the vortex shedding frequency and the velocity of the fluid.

$$S = \frac{fD}{U}$$

2.7.6 Vortex Shedding Frequency

Cycles of vortices shed per unit second is the vortex shedding frequency.

2.7.7 Aspect Ratio

Aspect ratio is defined as the width over the height of an object.

$$AR = \frac{W}{H}$$

2.8 Fluttering

2.8.1 Instability

If the oscillating fluid force tends to increase the vibration of the object, the structure is aerodynamically unstable and very large amplitude can result.

2.8.2 Fluttering

Torsion plunge instability of airfoil structures which is dynamic and static instability due to stalling is fluttering in airfoil structures. Fluttering occurs in stall region where the angle of attack exceeds the critical value of 15 degrees.

2.8.3 Galloping

One degree of freedom instability of bluff structure in civil engineering is known as galloping. For galloping, the value of reduced velocity should be less than 20 and the angle of attack less than 15 degrees.

2.9 Forces on the structure in the flowing fluid field

2.9.1 Drag Force

Force that is parallel but opposite in direction to the relative motion of the structure moving in a flowing fluid is known as drag force. It has direct relation with the velocity of the moving structure in the field.

$$F_D = \frac{1}{2}\rho(C_D V^2 A)$$

2.9.2 Lift force

Force that is perpendicular in direction to the oncoming flow direction is known as lift force. It usually acts in the upward direction.

Lift coefficient “CL” has direct relation with the angle of attack till it gets to the maximum. Beyond the critical angle of attack, the lift force starts dops.

CHAPTER 3: EXPERIMENTAL SETUP

We investigate the novel arrangement of an inverted flag in a wake of bluff body a circular cylinder to find the effect of voltage generation due to the deformation of the crystal lattice of a piezoelectric material in an open water tunnel as shown in a schematic. The piezoelectric flag (description: $\mathrm{DT2-028K/L}$) with material properties as shown in **Table 3-2** and details classification of material properties in **Table 3-1** is clamped between two acrylic bars and aligned with the incoming flow velocity with free leading edge and clamped trailing edge, bending rigidity β is varying from $0.001\ \mathrm{N.m}$ to $0.002\ \mathrm{N.m}$, velocities are varying from $0.17\mathrm{m/s}$ to $0.38\mathrm{m/s}$ and a gap $G_x = 0.5{\sim}3.0$.

Table 3-1: Mechanical and Electrical properties.

Symbol	Parameter		PVDF	Units
T	Thickness		9, 28, 52, 110	µm (micron, 10-6)
d31	Piezo Strain Constant		23	10-12
d33			-33	
g31	Piezo Stress constant		216	10-3
g33			-330	
k31	Electromechanical Coupling Factor		12%	
Kt			14%	
C	Capacitance		.com/.,mb380 for 28ìm	pF/cm2, @ 1KHz
Y	Young's Modulus		2-4	109 N/m2
V0	Speed of Sound	stretch:	1.5	103 m/s
		thickness:	2.2	
P	Pyroelectric Coefficient		30	10-6 C/m2 °K
Å	Permittivity		106-113	10-12 F/m
å/å 0	Relative Permittivity		12-13	
ρ_m	Mass Density		1.78	103kg/m
ρ_e	Volume Resistivity		>1013	Ohm meters
$R_\square$	Surface Metallization Resistivity		<3.0	Ohms/square for NiCu
$R_\square$			0.1	Ohms/square for Ag Ink
tan äe	Loss Tangent		0.02	@ 1KHz

Yield Strength	45-55	106 N/m2 (stretch axis)
Temperature Range	-40 to 80...100	$^{\circ}C$
Water Absorption	<0.02	% H2O
Maximum Operating Voltage	750 (30)	V/mil (V/µm), DC, @ 25°C
Breakdown Voltage	2000 (80)	V/mil (V/µm), DC, @ 25°C

Table 3-2: Material properties of an inverted piezoelectric flag

	Properties					
Material	**Young's Modulus**	**Poisson's ratio**	**Density**	**Height (Sheet)**	**Length (Sheet)**	**Diameter of Cylinder**
PVDF	E $= 1.38e^{9}Nm^{2}$	$v = 0.46$	$\rho_S = 0.96e^{3}kg - m^{3}$	H $= 16mm$	L $= 62mm$	$D = 25mm$

Note: All units are in SI

Parameter	**Units**	**Value**
Capacitance @ 1KHz	pF/m	600
Acoustic Impedance	MRayl	4.0
Relative Permittivity	@1KHz	9
tan ä$_e$	@1KHz	0.017
Hydrostatic Piezo Coefficient	pC/N Vm/N	15
Longitudinal Piezo Coefficient	Vm/N	250×10^{-3}
Hydrostatic Piezo Coefficient		150×10^{-3}
Electromechanical Coupling	%	20
Energy Output	mJ/Strain (%)	10
Voltage Output	kV/Strain (%)	5

Data Acquisition system used to measure a voltage generated from a piezo flag is DAQ (module in National Instrument lab view). Voltages are measure having a sampling rate=50 with a number of samples to read= 50 means in one second it measures 50 samples of voltages. After acquiring data from the DAQ assistant pass them to indicator, it will read in LabView and display as a number of charts for further processing (stored/ analyze).

Flag motion is recorded at 50 frames per second using a high-speed camera (Sony RX100 IV) mounted below the test section. Two flashlights on either side are used to illuminate the test section so as to increases the visibility of the flag. The experiment is performed in a water tunnel with a cross-section of the test section is 600×400cm, driven by a centrifugal pump capable of producing a flow velocity of $0.1 \sim 0.5$m/s. Flag length and height are 62mm and 16mm respectively.

Images are analyzed using image processing technique in MATLAB to determine the tale positioning of a flag in order to calculate peak to peak amplitude (A/L) and to create a superimposed view of the flag (flapping envelope). An experimental diagram of the inverted flag and aa circular cylinder in an open water tunnel along with a schematic diagram is shown in a figure.

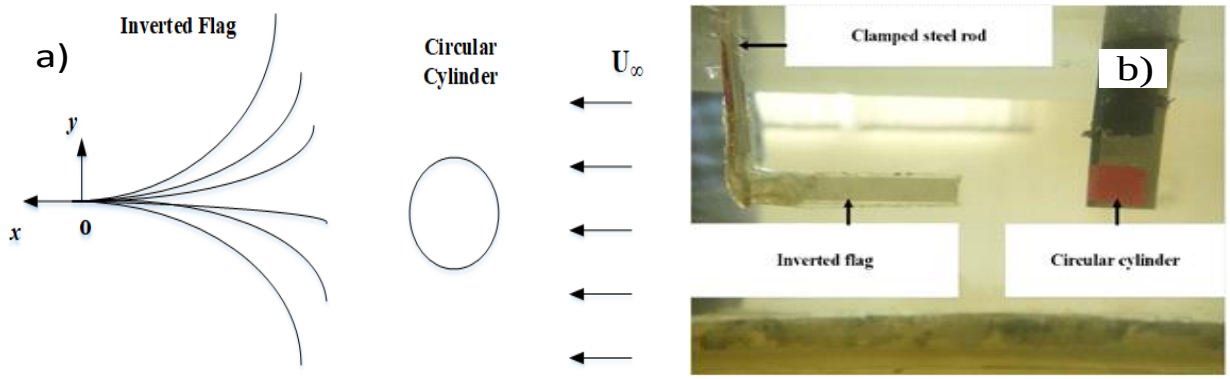

Figure 3-1: (a) Schematic (b) Piezoelectric flag and cylinder in a test section of water tunnel

A list of experiments is created based upon bending rigidity of material, Reynolds No. and streamwise gap. As three bending rigidity was used and on each bending rigidity combination of 36 configurations made as we have six different Reynolds No and six different streamwise gaps as well as shown in Table 3-3.

Figure related to water tunnel and equipment's used shown in Annex-1

Table 3-3: List of Experiments

	Flexural Rigidity (N.m)																	
	0.01						0.015						0.02					
S/D	0.5	1	1.5	2	2.5	3	0.5	1	1.5	2	2.5	3	0.5	1	1.5	2	2.5	3
Reynolds No.	4760	4760	4760	4760	4760	4760	4760	4760	4760	4760	4760	4760	4760	4760	4760	4760	4760	4760
	6160	6160	6160	6160	6160	6160	6160	6160	6160	6160	6160	6160	6160	6160	6160	6160	6160	6160
	7280	7280	7280	7280	7280	7280	7280	7280	7280	7280	7280	7280	7280	7280	7280	7280	7280	7280
	8400	8400	8400	8400	8400	8400	8400	8400	8400	8400	8400	8400	8400	8400	8400	8400	8400	8400
	9520	9520	9520	9520	9520	9520	9520	9520	9520	9520	9520	9520	9520	9520	9520	9520	9520	9520
	10624	10624	10624	10624	10624	10624	10624	10624	10624	10624	10624	10624	10624	10624	10624	10624	10624	10624

CHAPTER 4: RESULTS AND DISCUSSION

We investigated the flapping dynamics of inverted flag at different flexural rigidity ($0.001\text{N.m}^2 \sim 0.002\text{N.m}^2$), S/D ratio ($0.5 \sim 3.0$) and Reynolds number ranging from ($4760 \sim 10624$) in an open water tunnel at $\text{L/D} = 2$. In our case density and viscosity of water was used while diameter of a cylinder was fixed to 25mm so to avoid the effect of blockage, only velocity changes from $\text{v} = 0.017 \sim 0.38\text{m/s}$, below the velocity of 0.17m/s flow, is viscosity dominant so flag remains in a straight mode and maximum of 0.38m/s velocity was used as limitation to our experimental setup beyond that so much of vibration was produced in a tunnel results in a wake disturbance.

4.1 Effect of Reynolds no. and Streamwise gap on Vrms, A/L, and Flapping Frequency at $\gamma = 0.01$

In this case, bending rigidity γ of a flag was 0.001N.m^2 , flapping mode of flag was dependent upon a bending stiffness, flag exhibits straight mode at higher bending stiffness and flapping mode as bending stiffness decreases [17]. Tang stated that the inverted flag undergoes large instabilities due to either lift/drag force exerted on it that leads to a higher peak to peak amplitude and energy conversion. As shown in our case in fig.4-2(b) maximum flapping envelope (superimposed images) of an inverted flag for a gap (S/D ratio) and corresponding peak to peak amplitude with respect to time in fig.4-2(a). Point 1 indicates a maximum output voltage generated at a gap $G_x = 1.5$ and $\text{Re} = 10624$, maximum flapping frequency peak with an energy spectral density of 1.168×10^4 occur at same point as shown in fig4-3. As higher flapping frequency and peak to peak amplitude A/L causes higher voltage generation in a piezoelectric flag [14]. Similarly, in fig4-1(a) point 2 at the bottom shown a minimum voltage generation as it has been clear through the fig4-2(d) inverted flag envelope has a very low flapping. Fig4-1(b) and fig4-1(c) show a flapping frequency around 0.01 and A/L around 0.1 respectively.

In conventional flag as velocity increases flag flapping increases until it goes from periodic flapping to non-periodic flapping mode while in inverted flag as velocity increases it goes from periodic flapping mode to deflect mode [15] as indicated in a surface plot at a gap $G_x = 2.5 - 3.0$ and since in our case other factor constant in Reynolds no. was constant only velocity changes so at higher $\text{Re} = 9520 \sim 10624$ flag got deflected represents with a white color.

There was some region of interest in fig4-1(a) where considerable voltage generation. Specifically, at a gap $G_x = 1.0{\sim}2.0$ and a Re $= 9520{\sim}10624$. Flapping frequency of a flag and corresponding A/L has a high value over that range. As we move further toward a gap $G_x = 2.5{\sim}3.0$ shows a voltages drop due to the fact that flapping frequency was low causing less deformation [14].

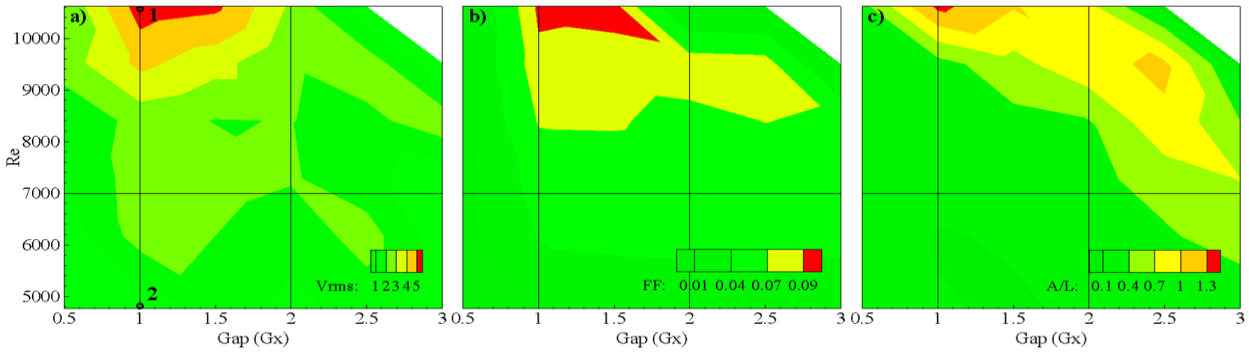

Figure 4-1: (a) Surface plot of root mean square voltage Vrms range from 1~5mV, point 1 indicate maximum Vrms of 5.53mV at Gx=1.0 & v=0.38m/s and point 2 indicates minimum Vrms of 0.165mV at Gx=1.0 & v=0.17m/s (b) Flapping frequency maximum of 0.09742 rads/sample at Gx=1.0 & range it from 0.01~0.098 (c) Peak-to-peak amplitude(A/L) maximum of 1.38 with range over 0.1~1.38.

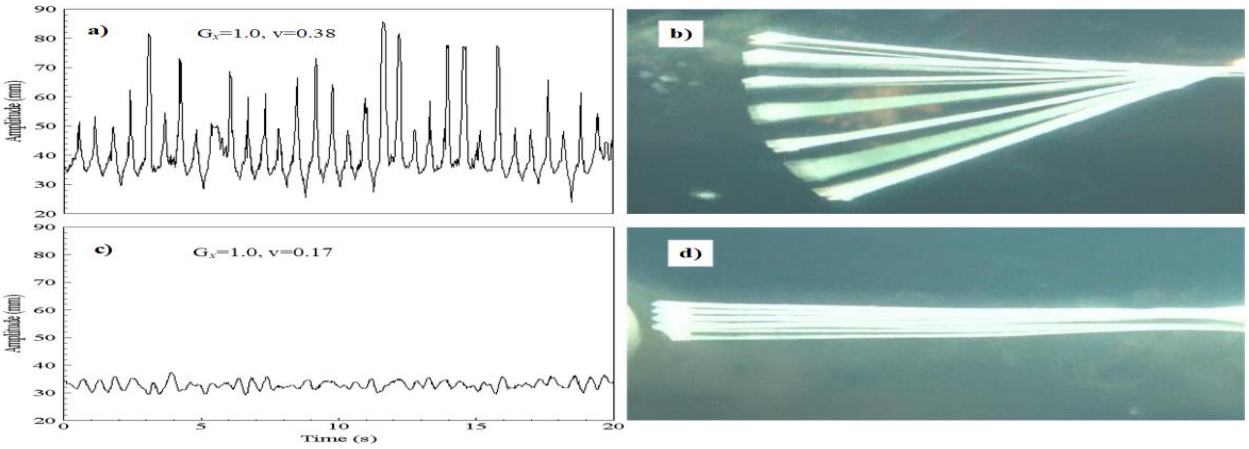

Figure 4-2: (a) tale positioning of maximum flapping case (b) superimposed views of image at Gx=1.0, v=0.38(c) tale positioning of minimum flapping (d) minimum envelope Gx= 1.0, v=0.17

Energy density of a signal using Fast Fourier Transform (FFT) in MATLAB was calculated for maximum and minimum flapping dominant frequency as shown in figure 4-3 and figure 4-4. It has been observed that the maximum spectral energy density of a dominant frequency occurs at bending rigidity of $\gamma = 0.01$.

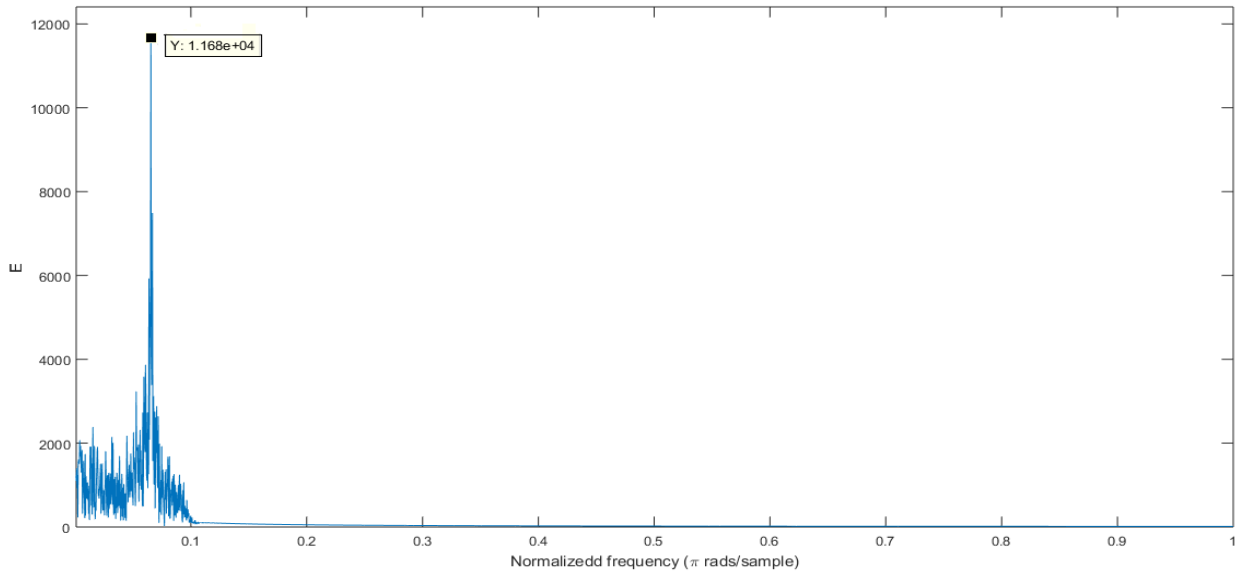

Figure 4-3: Energy density spectral of maximum flapping dominant frequency $\gamma = 0.01$

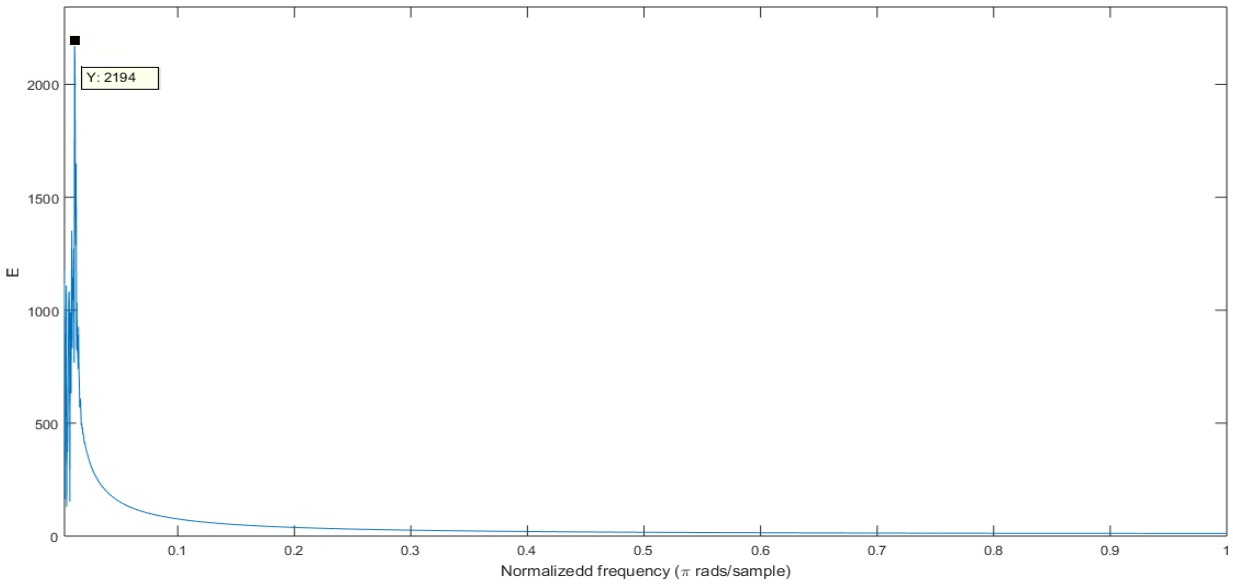

Figure 4-4: Energy density spectral of maximum flapping dominant frequency $\gamma = 0.01$

4.2 Effect of Reynolds no. and Streamwise gap on Vrms, A/L, and Flapping Frequency at $\gamma = 0.015$

In that scenario varying bending rigidity γ from 0.001N.m^2 to 0.0015N.m^2, increasing flexural rigidity making it stiffer so more drag force required to flap [26] thus root mean square voltage (Vrms) has of less generation. As shown in fig4-6(b), the flag has tilted more on the left extreme as it got stiffer and then starts flap there. However, peak to peak amplitude has good range over a period and a maximum $\text{A/L} = 1.28$. In fig4-5(a) point 1 indicates maximum voltage

generated, as flapping frequency got maximum peak with energy density of 1.128×10^4 shown in fig4-7. Ryu stated that large peak to peak amplitude results in high curvature thus leads to large mean strain energy. Since maximum peak to peak amplitude occurs at that point so results in a higher voltage generation as shown in fig4-5(c). Fig4-6(b) and fig4-6(d) show the maximum and minimum envelope of flag with corresponding tail positioning in fig4-6(a) and fig4-5(c).In a gap between $G_x = 0.5{\sim}1.50$ flag has shown a higher flapping frequency range and goes a maximum of 0.07 at a $\mathrm{Re} = 10624$ and $G_x = 1.0{\sim}1.50$ and corresponding higher peak to peak amplitude of a flag causing large mechanical strain energy conversion into electrical energy.

Contrary point 2 on fig4-5(a) has a minimum of Vrms, as shown in a flapping frequency surface plot flag flaps with a lower frequency and peak to peak amplitude of flag is lower as well as shown in fig4-5(b) and fig4-5(c). Since the flag is so closed to the cylinder so fluid drag viscous force is not that strong to make a flag to flap properly as a result in slight motion. Flapping frequency and peak to peak amplitude (A/L) in fig4-5(b) and fig4-5(c) affirm as it has a value of 0.01 and less than 0.1 respectively. Voltage show considerable good value in a gap $G_x = 1.0{\sim}2.0$ and Reynolds no. values ranging from $\mathrm{Re} = 7280{\sim}9520$ as shown in fig4-5(a). As dominant frequency and peak to peak amplitude (A/L) value has a higher value in that range, Tang stated that as in a flapping regime at larger (A/L) flag frontal area increases when reached maximum displacement and thus large value of incoming drag/lift force induced on a flag results in energy conversion. So, this leads to a high value of Vrms as shown in fig4-5(a)

Flapping frequency decrease with the increase of bending stiffness and it is observed that flag goes from periodic flapping mode to deflected mode [26] as shown in fig4-a when the velocity increases and at $G_x = 2.0{\sim}3.0$ flag starts to deflect. At gap $G_x = 2.0$ it occurs at a maximum Reynolds no while at a gap $G_x = 2.5$ & 3.0 it's range increases and it deflects at $\mathrm{Re} = 8400{\sim}10624$.

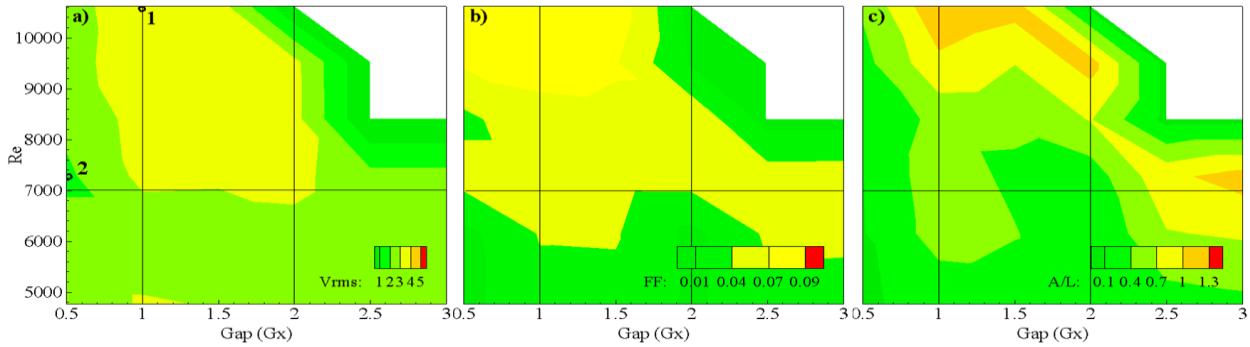

Figure 4-5:(a) Surface plot of root mean square voltage Vrms range from 1~5mV, point 1 indicate maximum Vrms of 3.4mV at Gx=1.0 & v=0.38m/s and point 2 indicates minimum Vrms of 1.79mV at Gx=1.0 & v=0.17m/s (b) Flapping frequency maximum of 0.08932 rads/sample at Gx=1.0 (c) Peak-to-peak amplitude(A/L) maximum of 1.26 with range over 0.1~1.3

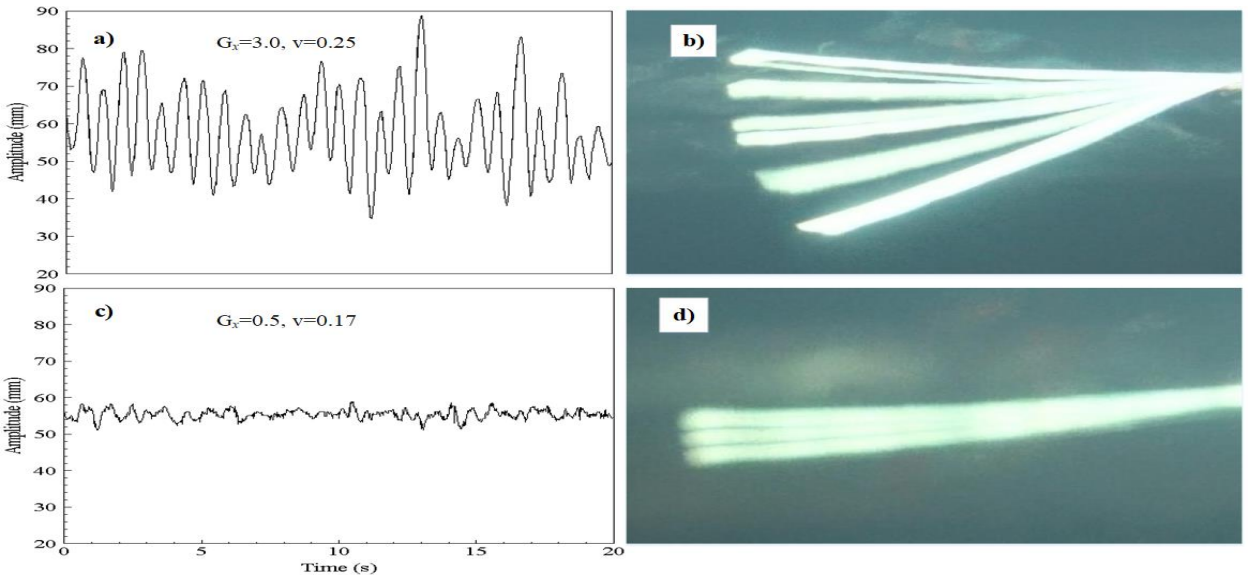

Figure 4-6: (a) tale positioning of maximum flapping case (b) maximum envelope Gx=3.0, v=0.25(c) tale positioning of minimum flapping (d) minimum envelope Gx= 0.5, v=0.17

Energy density of a signal using Fast Fourier Transform (FFT) in MATLAB was calculated for maximum and minimum flapping dominant frequency as shown in figure 4-7 and figure 4-8. It has been observed that maximum spectral energy density of a dominant frequency $\gamma = 0.015$ was 1.128×10^4 and minimum spectral density was 1696.

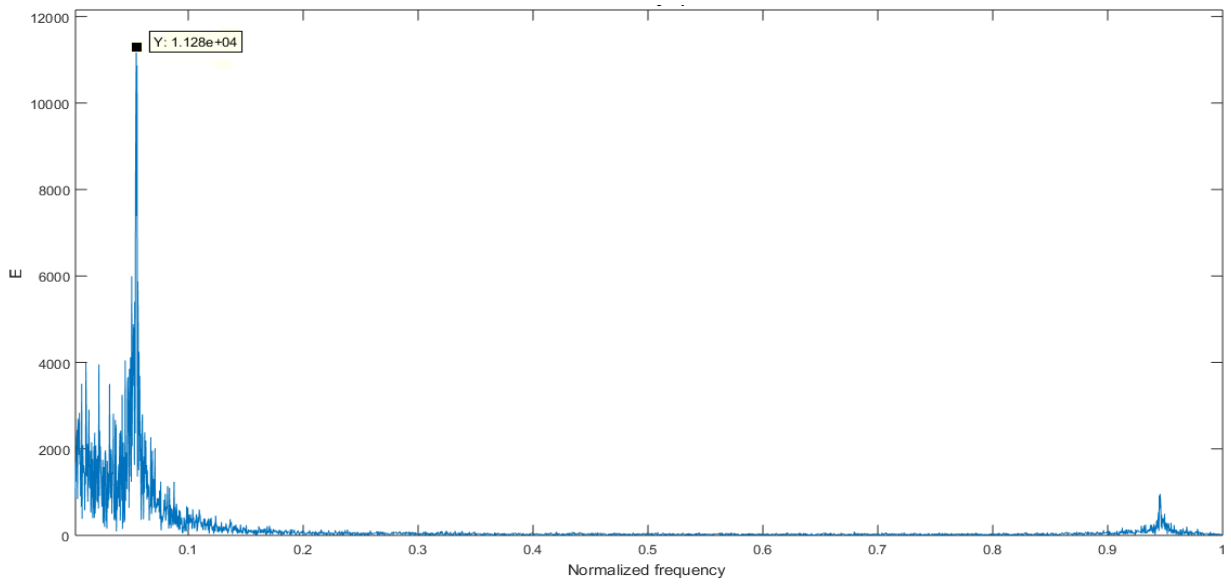

Figure 4-7: Energy Spectral density of maximum flapping dominant frequency at $\gamma = 0.015$

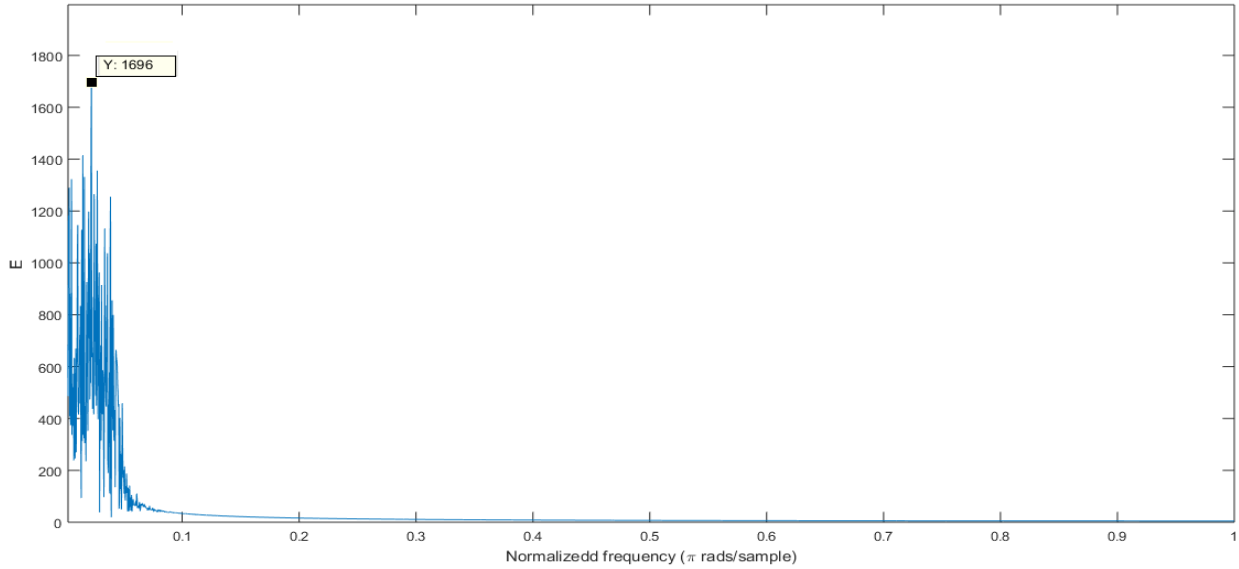

Figure 4-8: Energy Spectral density of minimum flapping dominant frequency at $\gamma = 0.015$

4.3 Effect of Reynolds no. and Streamwise gap on Vrms, A/L, and Flapping Frequency at $\gamma = 0.02$

In that case, bending rigidity γ is 0.002N.m^2, it has been observed that maximum voltage generation Vrms is less than the previous two cases. However, peak to peak amplitude here is a little less than the previous scenario as shown in fig6-c. Point 1 in fig4-9(a) showed maximum voltage generated, flapping frequency compared to the above mentioned case is lower with energy density of 1.125×10^4 as increasing bending stiffness lower will be a fluttering [26]. Fig4-10(b) and fig4-10(d) show minimum and maximum superimposed view of images as flag frontal area

increases shown in fig4-10(b) dynamic pressure induced on a flag increases with the increase of flow velocity thus results in an increased peak to peak amplitude [27]. It prolongs over a gap $G_x = 1.0 \sim 2.0$ and flag shows higher flapping frequency range as well as a voltages Vrms.

Point 2 in fig4-9(a) indicates minimum Vrms, it occurs at $G_x = 0.5$ as flag is close to bluff body flag frontal area exposed to incoming flow is low as shown in fig4-10(d) a low flapping envelope thus less dynamic pressure exerted on a flag results in low peak to peak amplitude [27]. and when the incoming flow velocity is low flag remains in an undeformed mode [15]. As at that point flow velocity is low i.e. $v = 0.17 m/s$ agrees with the statement of [15] Fig4-9(b) and fig4-9(c) affirm a low flapping frequency and peak to peak amplitude.

There was a transition region from no or low voltage generation to peak point voltage generation as highlighted by the light yellowish region. Like the other two cases, there were some regions in that scenario where the flag got deflected marked with a white region. As the Reynolds no. increases at a gap $G_x = 2.0 \sim 3.0$ flapping frequency decrease due to an increase in a bending stiffness [26] results in a change in mode from periodic flapping to deflected mode. At gap $G_x = 2.0$ it occurs at a higher Reynolds No. while at a gap $G_x = 2.5$ & 3.0 it's range increases and it deflects at $\mathrm{Re} = 8400 \sim 10624$.

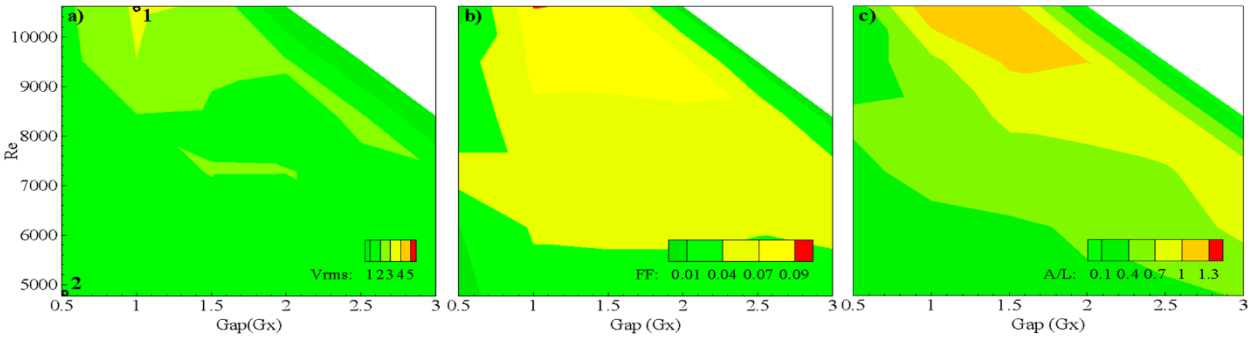

Figure 4-9: (a) Surface plot of root mean square voltage Vrms range from 1~5mV, point 1 indicate maximum Vrms of 3V at Gx=1.0 & v=0.38m/s and point 2 indicates minimum Vrms of 1.18mV at Gx=0.5 & v=0.17m/s (b) Flapping frequency maximum of 0.08797 rads/sample at Gx=1.0 (c) Peak-to-peak amplitude(A/L) maximum of 1.25 with range over 0.1~1.3

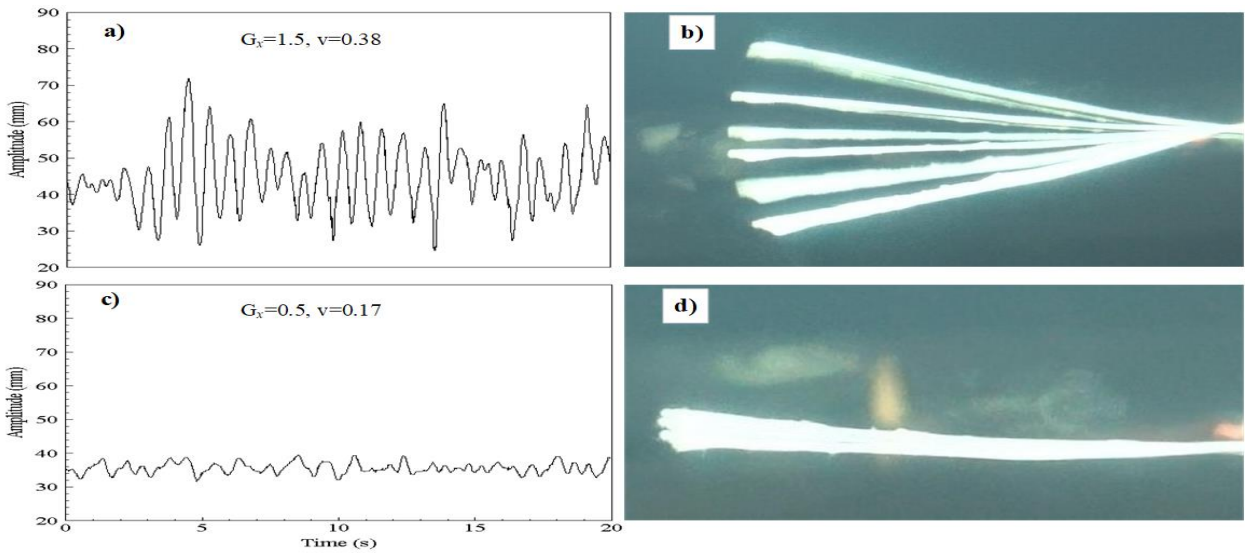

Figure 4-10: (a) tale positioning of maximum flapping case (b) maximum envelope Gx=1.5, v=0.38(c) tale positioning of minimum flapping (d) minimum envelope Gx= 0.5, v=0.17m/s

Energy density of a signal using Fast Fourier Transform (FFT) in MATLAB was calculated for maximum and minimum flapping dominant frequency as shown in figure 4-11 and figure 4-12. It has been observed that maximum spectral energy density of a dominant frequency $\gamma = 0.02$ was 1.125×10^4 and minimum spectral density was 1064.

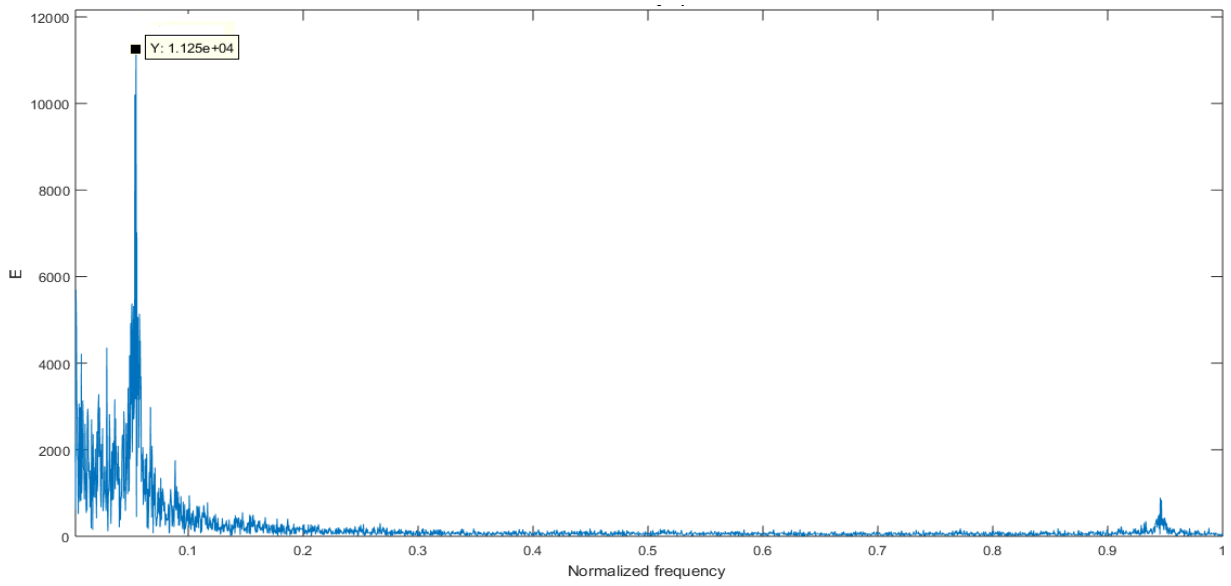

Figure 4-11: Energy Spectral density of maximum flapping dominant frequency at $\gamma = 0.02$

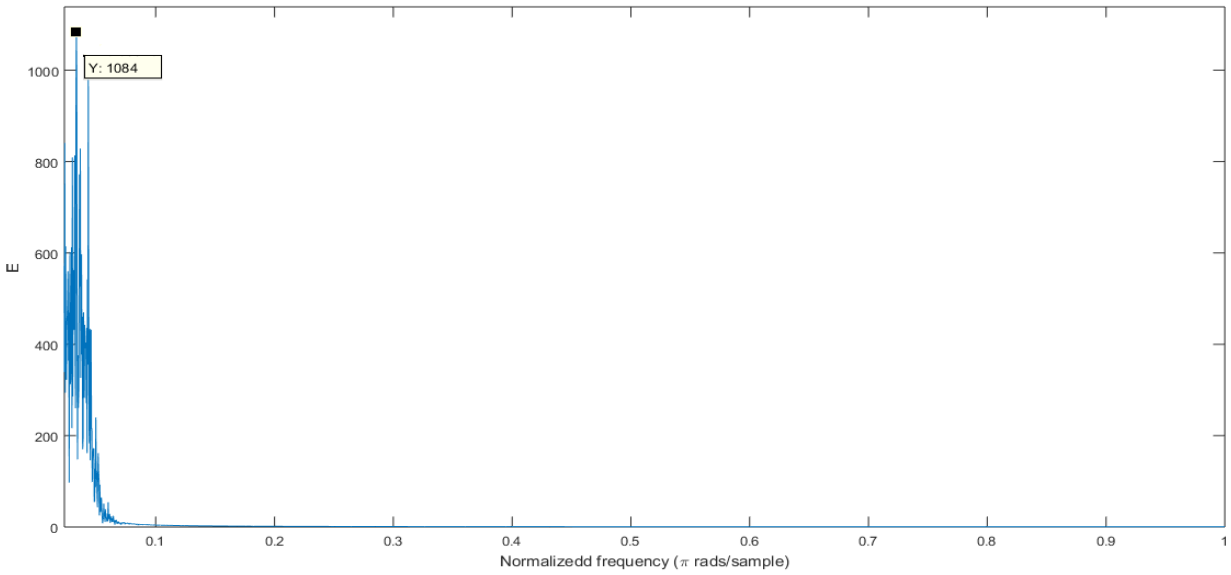

Figure 4-12: Energy Spectral density of minimum flapping dominant frequency at $\gamma = 0.02$

4.4 Effect of Reynolds no. and Streamwise gap comparison at all flexural rigidity γ

As bending rigidity γ was changed from 0.001N.m^2 to 0.002N.m^2 its effect's the dynamics of flapping, increasing bending rigidity γ as shown in surface plot of flapping frequency the dominant frequency tends to decrease with the increase of bending stiffness [26]. Apart from γ other factors like Reynolds No. effect the deformation of ca rystal lattice, so we get a different behavior of voltage generation Vrms.

The region of all cases where voltage generation Vrms is maximum is at a gap $G_x = 1.0\sim2.0$, as there are three regions of boundary layer formation near wake, Kolmogorov region and then deformed state, as at $G_x = 1.0\sim2.0$ it lies in a fully developed region (Kolmogorov) after that spectrum energy gets low and vortices energy starts to dissipate. Thus, voltage Vrms didn't get a maximum peak over there.

At $\gamma = 0.001\text{N.m}$ we got maximum V_{rms} at a Reynolds No. range above $9000\sim10000$. Reynolds no. below 9000 we got minimal voltages as dominant frequencies are low and it is dominant by flow viscosity V_{rms} is maximum is at a gap $G_x = 1.0\sim2.0$ as it lies in a fully developed region (Kolmogorov) Maximum voltage generated in a case where $\gamma = 0.001\text{N.m}$ as at that point both the flapping frequency (dominant frequency) and peak to peak amplitudes were high.

At $\gamma = 0.0015\text{N.m}$ as we reach Reynolds No. of 7000 we got V_{rms} of above 3mV and remains consistent till above 10000 for a streamwise gap $G_x = 1.0 \sim 2.0$. As flapping frequency shows a wider range of Reynolds No. above $6000 \sim 10000$ and for all streamwise gap at 7000 and at streamwise gap between $1 \sim 2$ for larger values of Reynold no.

At $\gamma = 0.002\text{N.m}$ we only get maximum $V_{rms} = 3\text{mV}$ at Reynolds no. above 10000 and it only occurs at streamwise gap $G_x = 1.0$.Below Reynolds no. < 10000 for all streamwise gap we got low to minimal voltages. Although we got flapping frequency since the structure is so stiff it not been able to convert mechanical strain energy into electrical energy. Amplitude over active length A/L the region remains the same for all flexural rigidity γ cases Reynold no.

Maximum voltage generated in a case where $\gamma = 0.001\text{N.m}^2$ as at that point, both the flapping frequency(dominant frequency) and peak to peak amplitudes are high thus as [27] stated at high A/L and in extreme position flag frontal area increases so fluid dynamic pressure exerted on a flag increases thus large instability induced on a flag due to either lift/drag force leads to high energy conversion[17]. Common region of all the cases occur at a gap $G_x = 3.0$ and a higher $\text{Re} = 10624$ where flag got deflected as stated in inverted flag configuration increase in velocity flag entered in a deflected mode from periodic flapping mode [15] .

Although, in case 1 just a slight inclination of flag on a left side we got a maximum peak to peak amplitude as in a flapping frequency surface plot reflects it got the highest peak of dominant frequency but with lower energy density E occur in that case. Figures related to voltage and completed envelope shown in Annex-2.

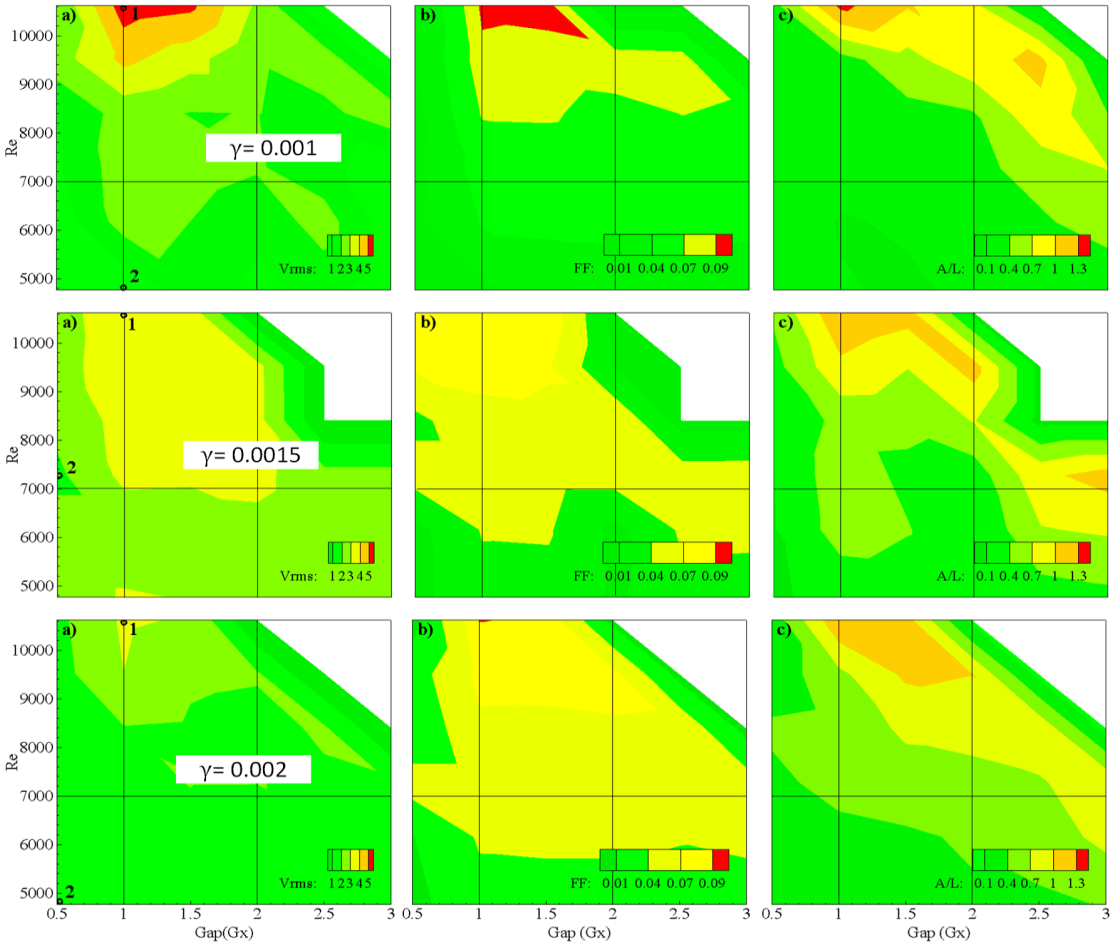

Figure 4-13: Overall response at $\gamma = 0.001\text{N.m}, \gamma = 0.0015\text{N.m}$ and $\gamma = 0.002\text{N.m}$, on all parameters i.e. root mean square Voltage Vrms , Flapping frequency of flag and peak to peak amplitude over a length of flag (A/L)

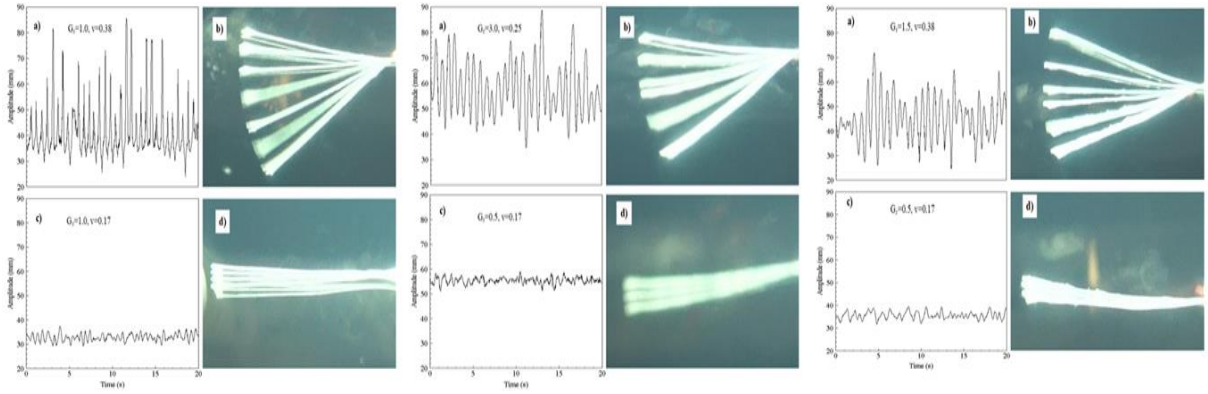

Figure 4-14: Maximum and minimum flapping envelope (superimposed images) and tail positioning of inverted flag at $\gamma = 0.001\text{N.m}, \gamma = 0.0015\text{N.m}$ and $\gamma = 0.002\text{N.m}$

4.5 PIV Results

Particle image velocimetry technique was used to study the dynamics of vortex formed at the downstream of bluff body. As circular cylinder was used to generate alternating vortices at their downstream and to study their impact on a piezoelectric eel, their interaction with a flag and to study the constructive and destructive interferences with a flag.

Selecting three cases of maximum peak to peak amplitude (A/L) at three different flexural rigidity. By performing PIV at the downstream of bluff body and at the downstream of inverted flag as shown in annex-3.

Figure 7-1 in annex-3 shows speed and vorticity surface plot at the downstream of inverted flag at flexural rigidity $\gamma = 0.001\, N.m.$ Velocity surface plot shows at the downstream of inverted flag while moving in a streamwise gap streamlines was formed and velocity reaches maximum speed of 0.24m/s while vorticity surface plot show similar behavior means it lies in a non-vortex region shown by a green color so that streamlines was formed, and flow was uniform again.

Figure 7-2 in annex-3 shows speed and vorticity surface plot at the downstream of bluff body (circular cylinder) at flexural rigidity $\gamma = 0.001\, N.m.$ Velocity surface plot shows at the downstream of circular cylinder while moving in a streamwise gap alternating vortices was formed that impart their energy on an inverted flag, vortex formed from right tend to move a flag in downward direction while vortex formed from left of a bluff body tend to move the flag a in upward direction so as they impart their energy on a flag, flag starts to flap in periodic manner. Von Karman Street was formed as the alternating vortices starts to shed. When both the vortex was in same direction constructive interference occur and the flapping of flag reaches maximum amplitude, similarly when both the vortex was in opposite direction destructive interference occur results in a minimum amplitude of flag. Figure 7-3, 7-4 shows particle image velocimetry surface plot at downstream of bluff body and at downstream of inverted flag at flexural rigidity $\gamma = 0.0015\, N.m$ and figure 7-5, 7-6 shows particle image velocimetry surface plot at downstream of bluff body and at downstream of inverted flag at flexural rigidity $\gamma = 0.002\, N.m.$ Figure 7-7 shows combine vorticity surface plot at $\gamma = 0.001\, N.m$, $\gamma = 0.0015\, N.m$, $\gamma = 0.002\, N.m$ in Annex-3.

4.6 CONCLUSION

In this study, we analyzed the dynamics of a piezoelectric flag in an inverted configuration and its effect on energy harvesting. It has been observed that bending stiffness has its impact on energy harvesting from the piezoelectric flag. In three different cases based on bending rigidity and 36 different combinations in every case, V_{rms} has been calculated. It has been observed that maximum voltage in all three cases occur in a gap between $G_x = 1.0 \sim 2.0$ and at a higher $\mathrm{Re} = 10624$. Furthermore, flapping dynamics play its vital role in energy harvesting, as flapping frequency and peak to peak amplitude $(\mathrm{A/L})$ both are high in case 1 so we got maximum of a voltage generation among all three cases. It has been observed that maximum energy density occurs at $\gamma = 0.001\ \mathrm{N.m^2}$ and in scenario 2 voltage generation at lower Reynolds no. remains in a constant range of 2~3mV better than the remaining two scenarios. It has also observed flag got deflected at higher velocity at a gap range between $G_x = 2.0 \sim 3.0$ in all cases due to larger instabilities in inverted flag it goes into deflected mode from periodic flapping mode. It has been found out that increases bending stiffness flapping frequency, peak to peak amplitude and the root means square voltage V_{rms} decrease.

Annex-1

Experimental Figures

Figure 5-1: Test Section of Water Tunnel

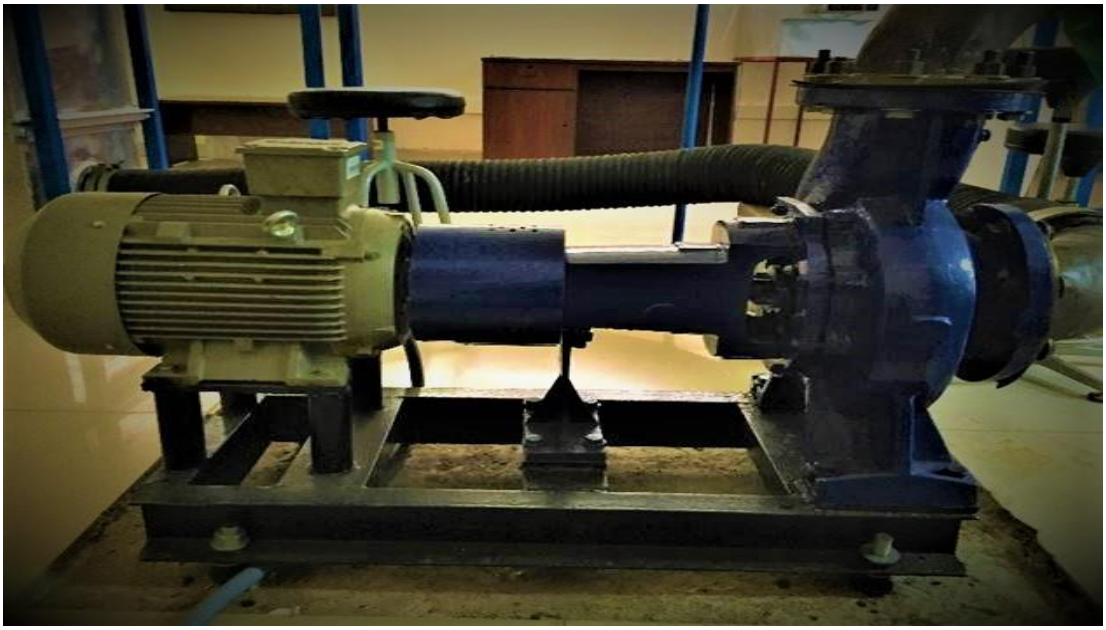

Figure 5-2: Centrifugal Pump for circulating water in a test section

Figure 5-3: Piezoelectric EEL

Figure 5-4: High Speed Camera for capturing flapping motion of eel

Figure 5-5: Deck Card for attaining analog voltage signal from flapping motion of piezoelectric eel

Figure 5-6: LED flashlight for illuminating Test Section

Annex-2

Voltage Result Figures

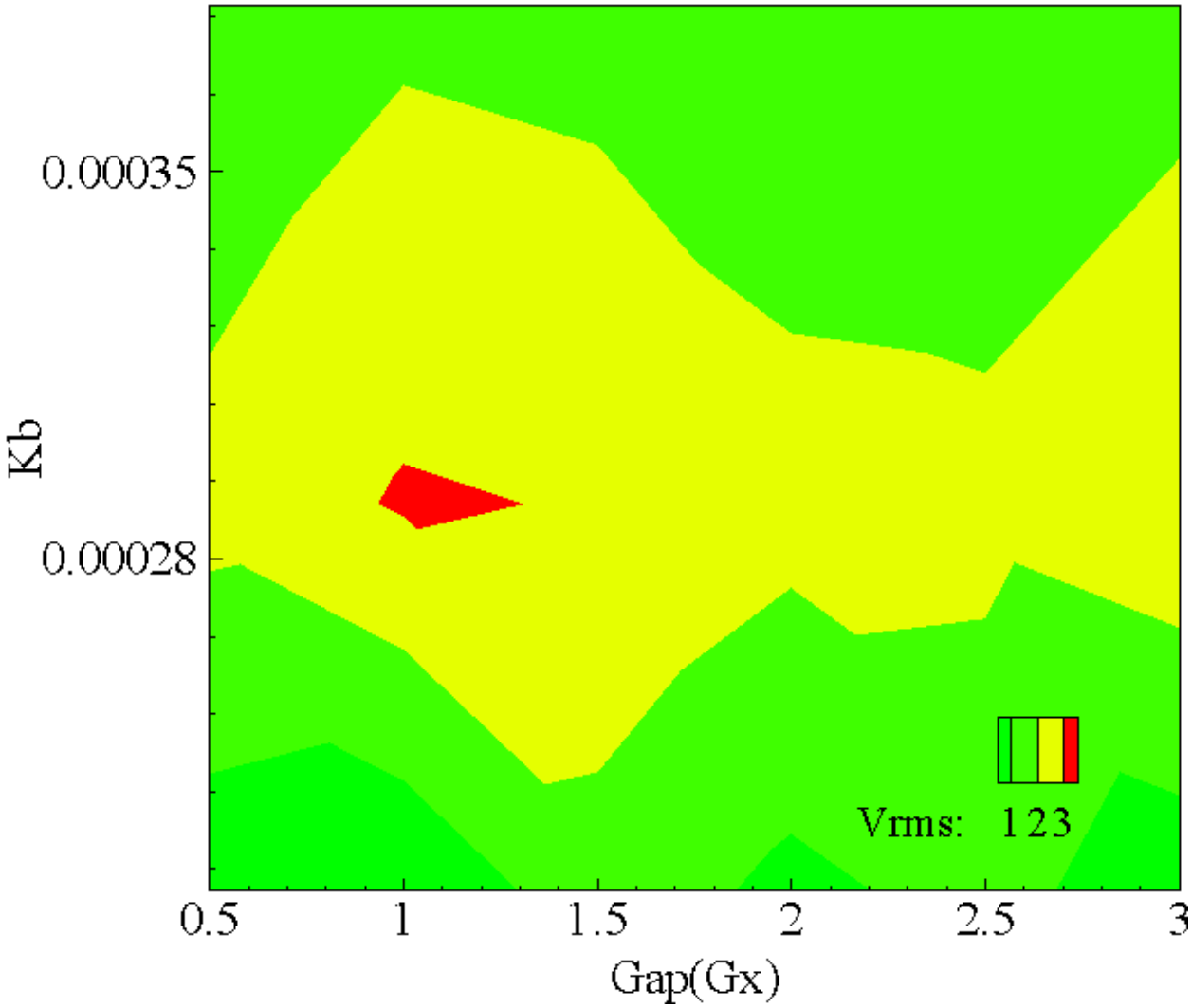

Figure 6-1: Bending Stiffness vs Streamwise gap

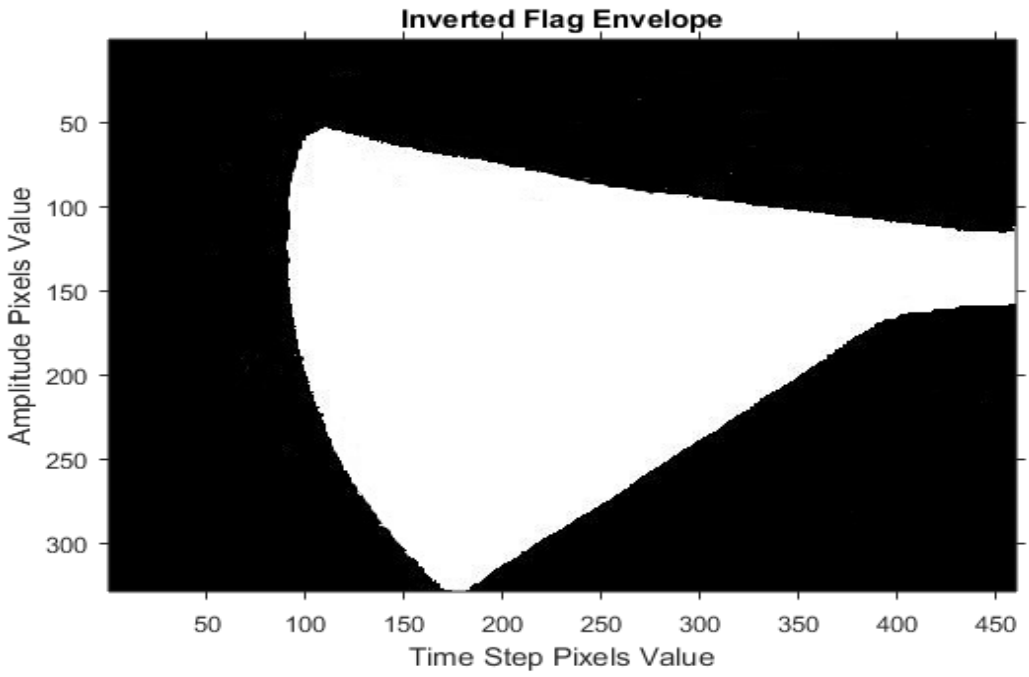

Figure 6-2: Complete Flapping Envelope of inverted flag at $\gamma = 0.01$

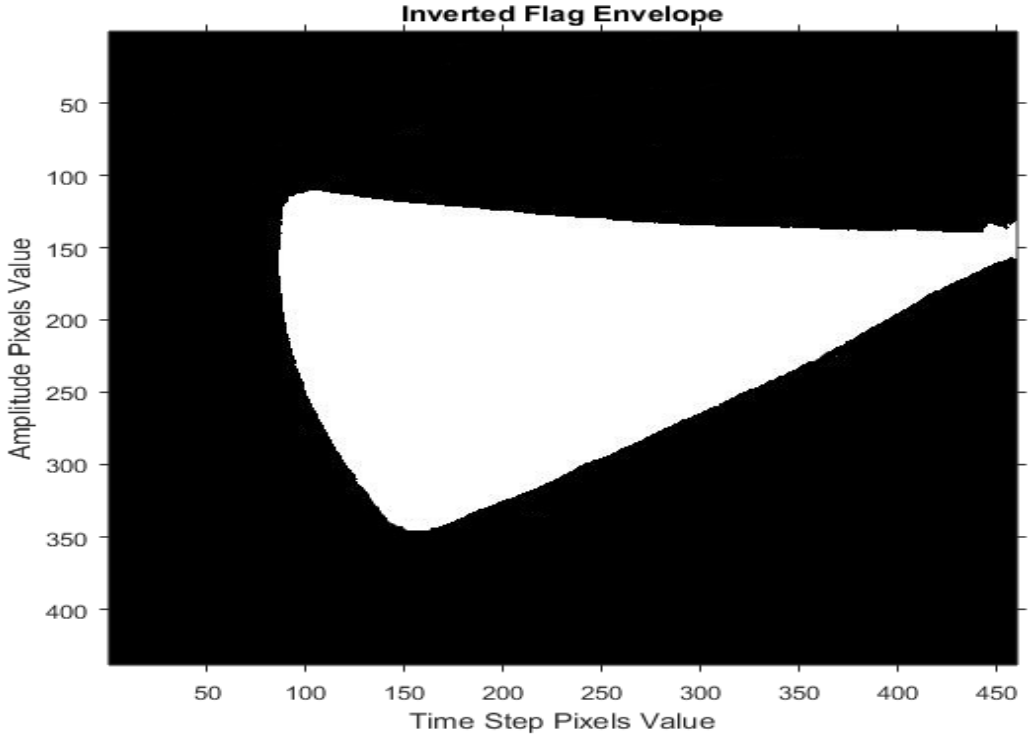

Figure 6-3: Complete Flapping Envelope of inverted flag at $\gamma = 0.015$

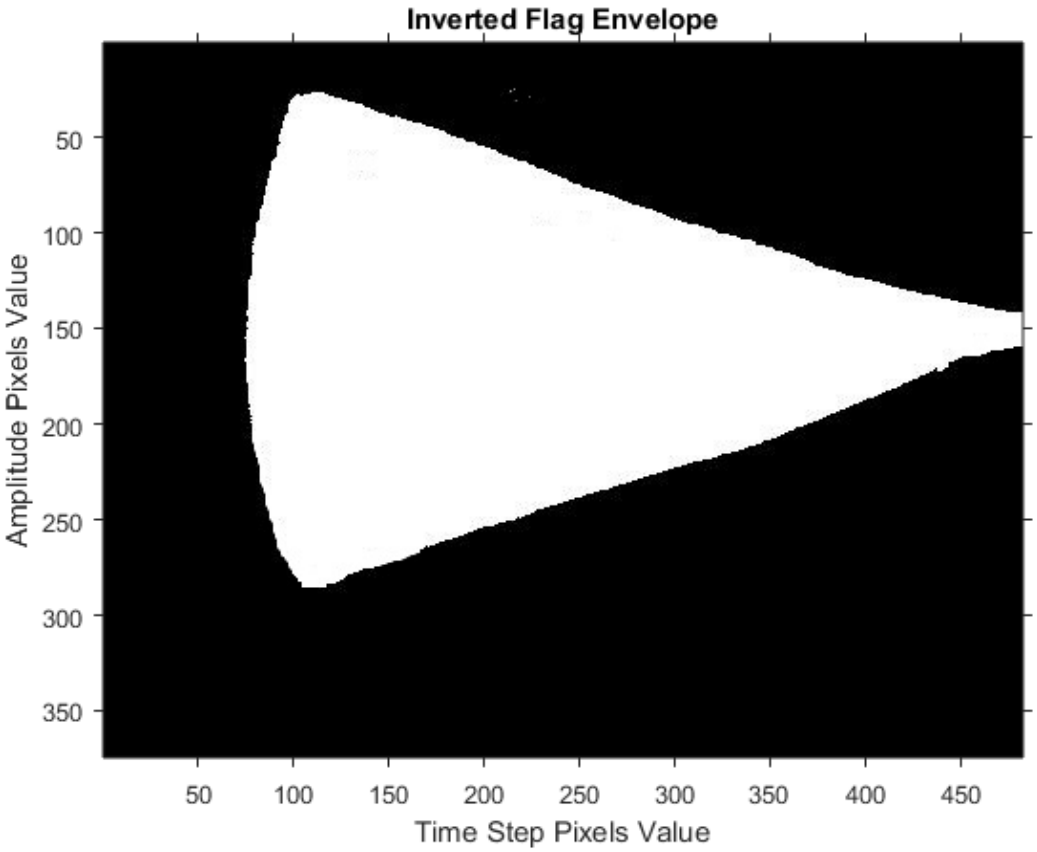

Figure 6-4: Complete Flapping Envelope of inverted flag at $\gamma = 0.02$

Annex-3

Particle Image Velocimetry (PIV) results figure

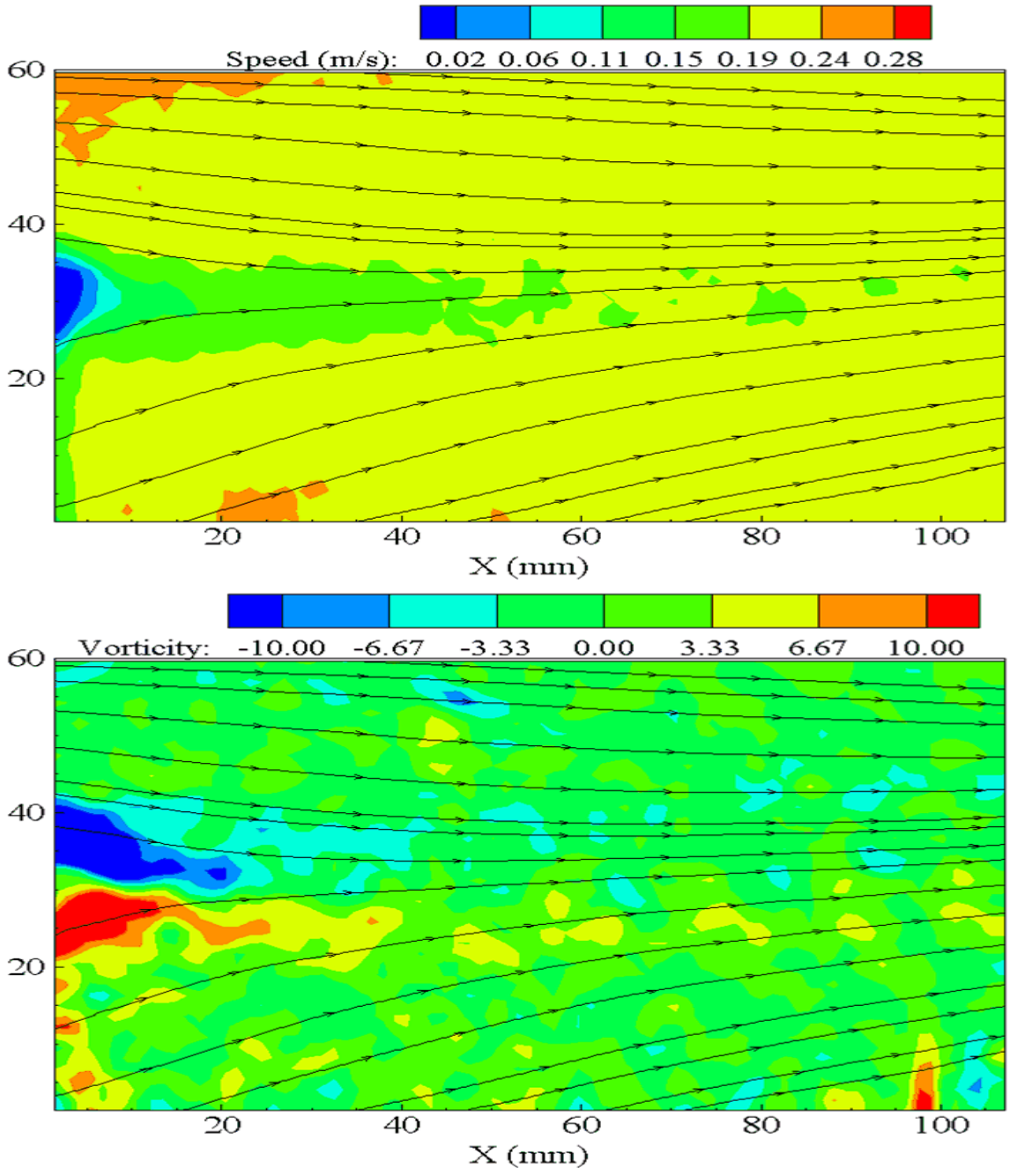

Figure 7-1: Flow field and vorticity plot at a downstream of inverted flag

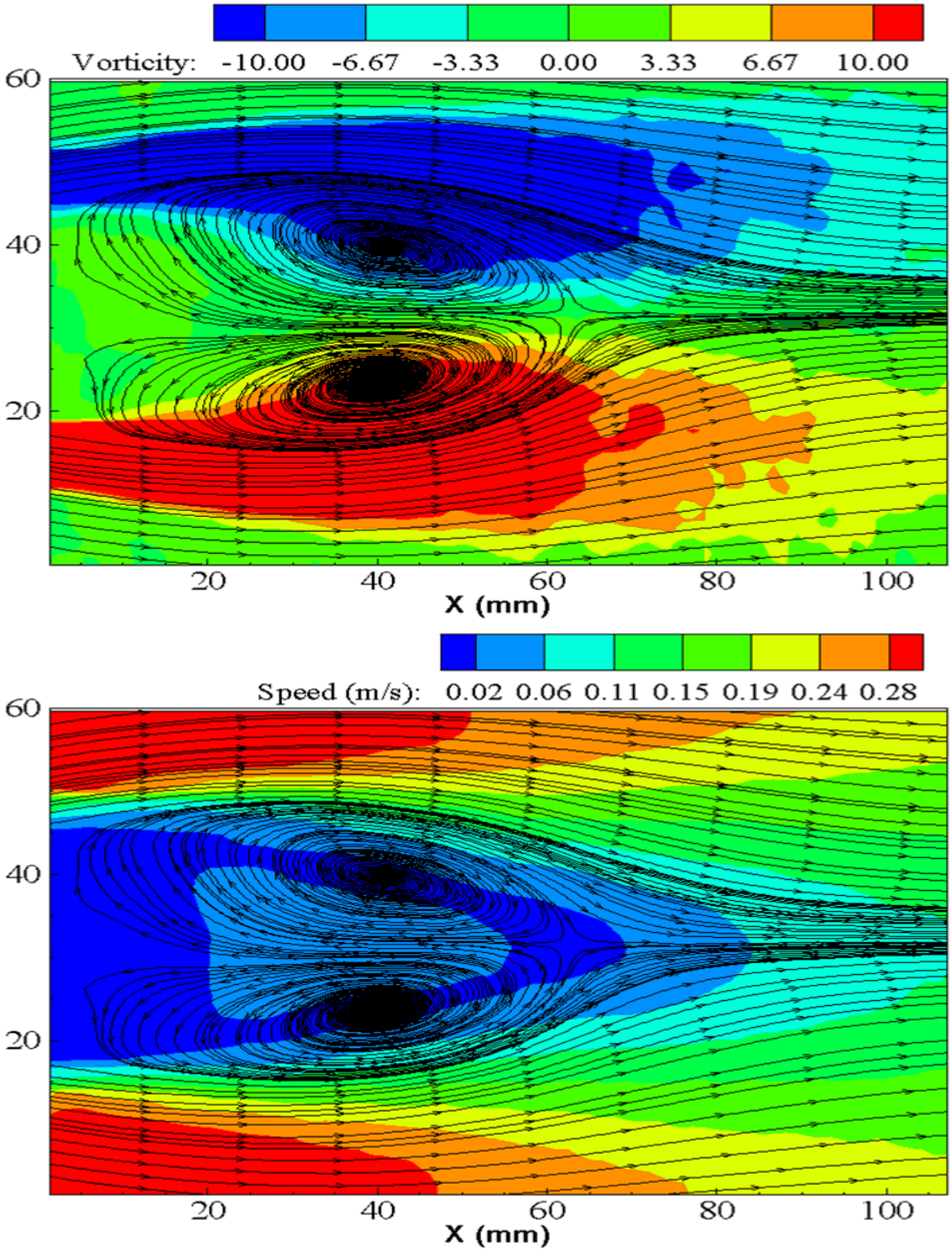

Figure 7-2: Flow field and vorticity plot at a downstream of bluff body

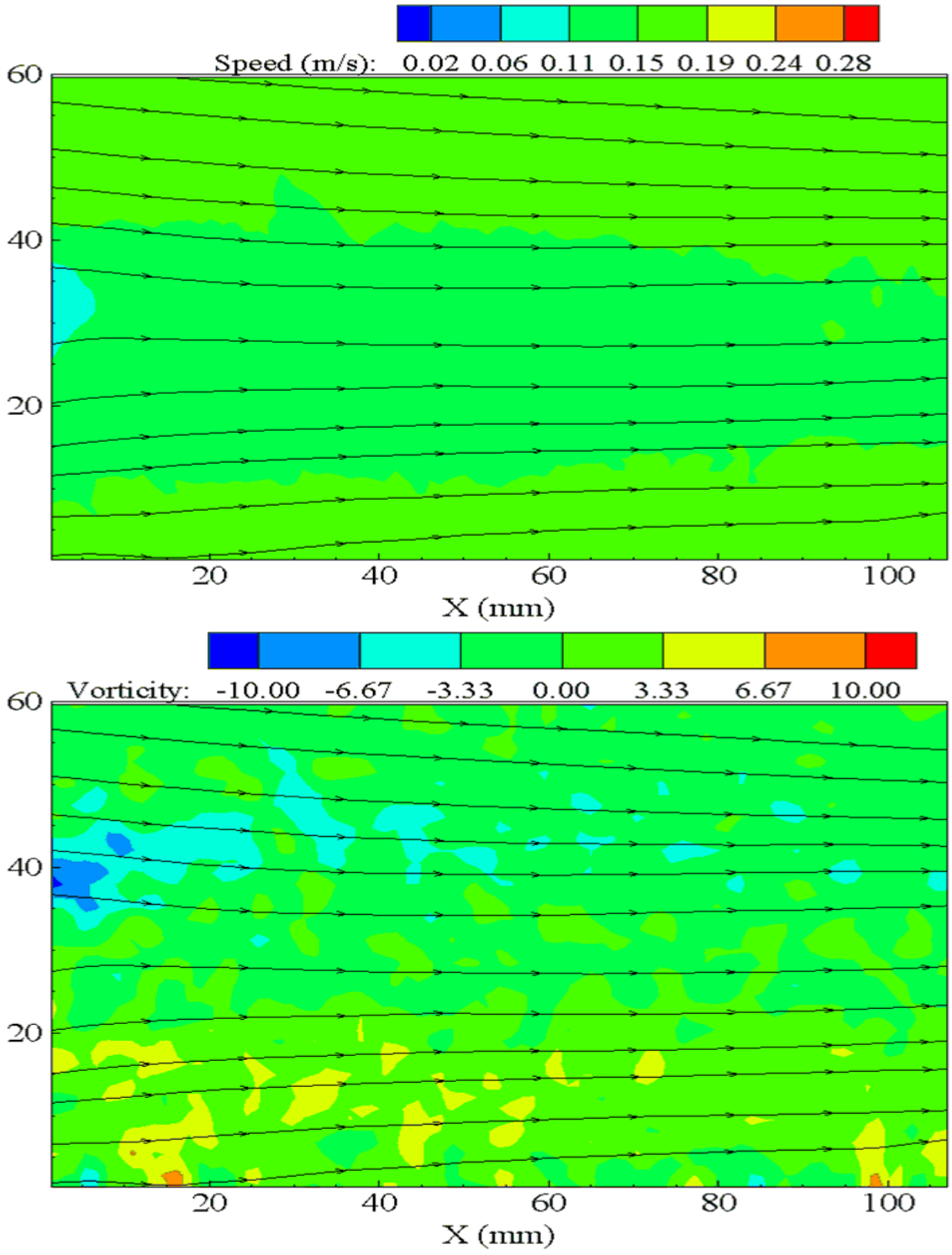

Figure 7-3: Flow field and vorticity plot at a downstream of inverted flag at

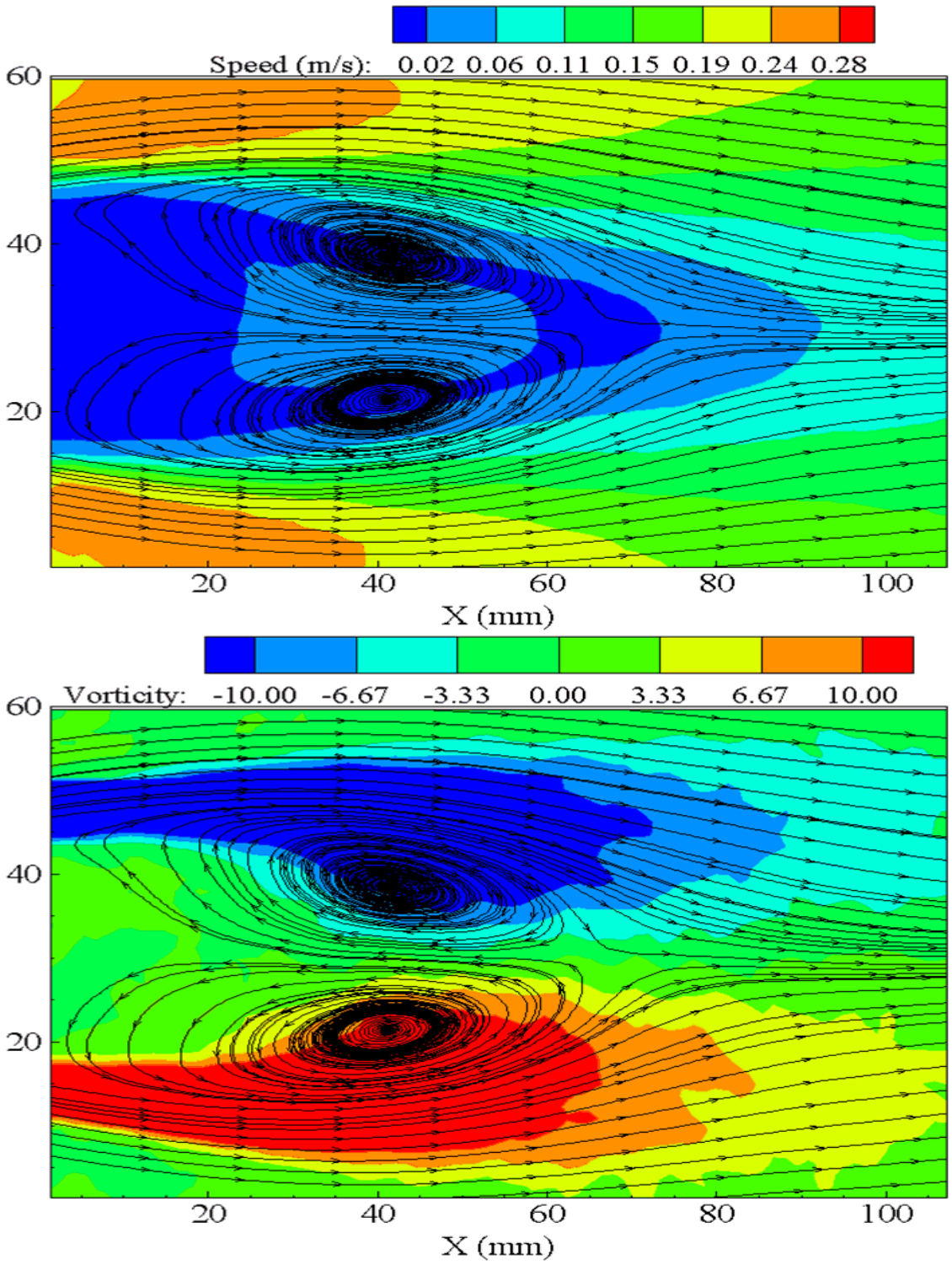

Figure 7-4: Flow field and vorticity plot at a downstream of bluff body

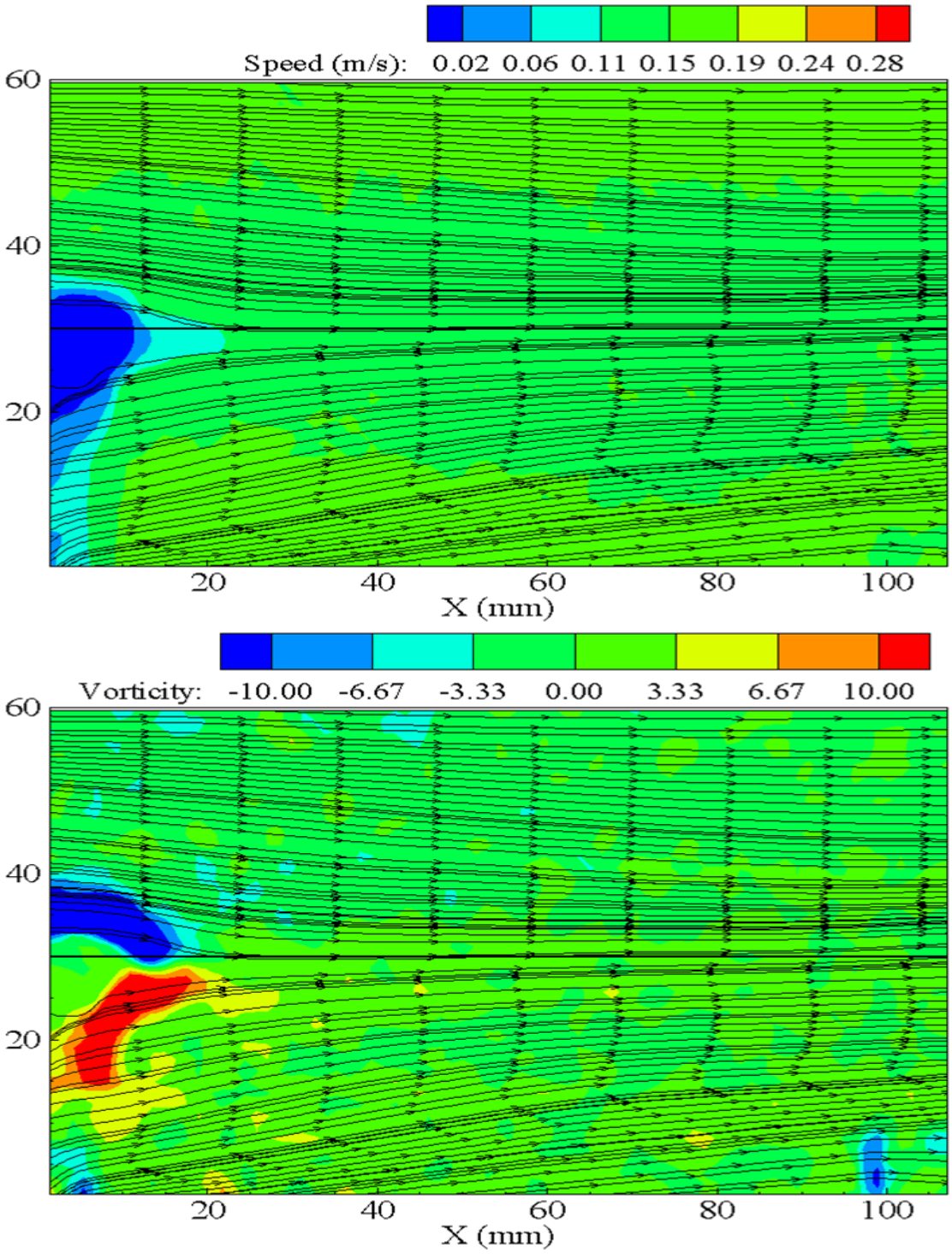

Figure 7-5: Flow field and vorticity plot at a downstream of inverted flag

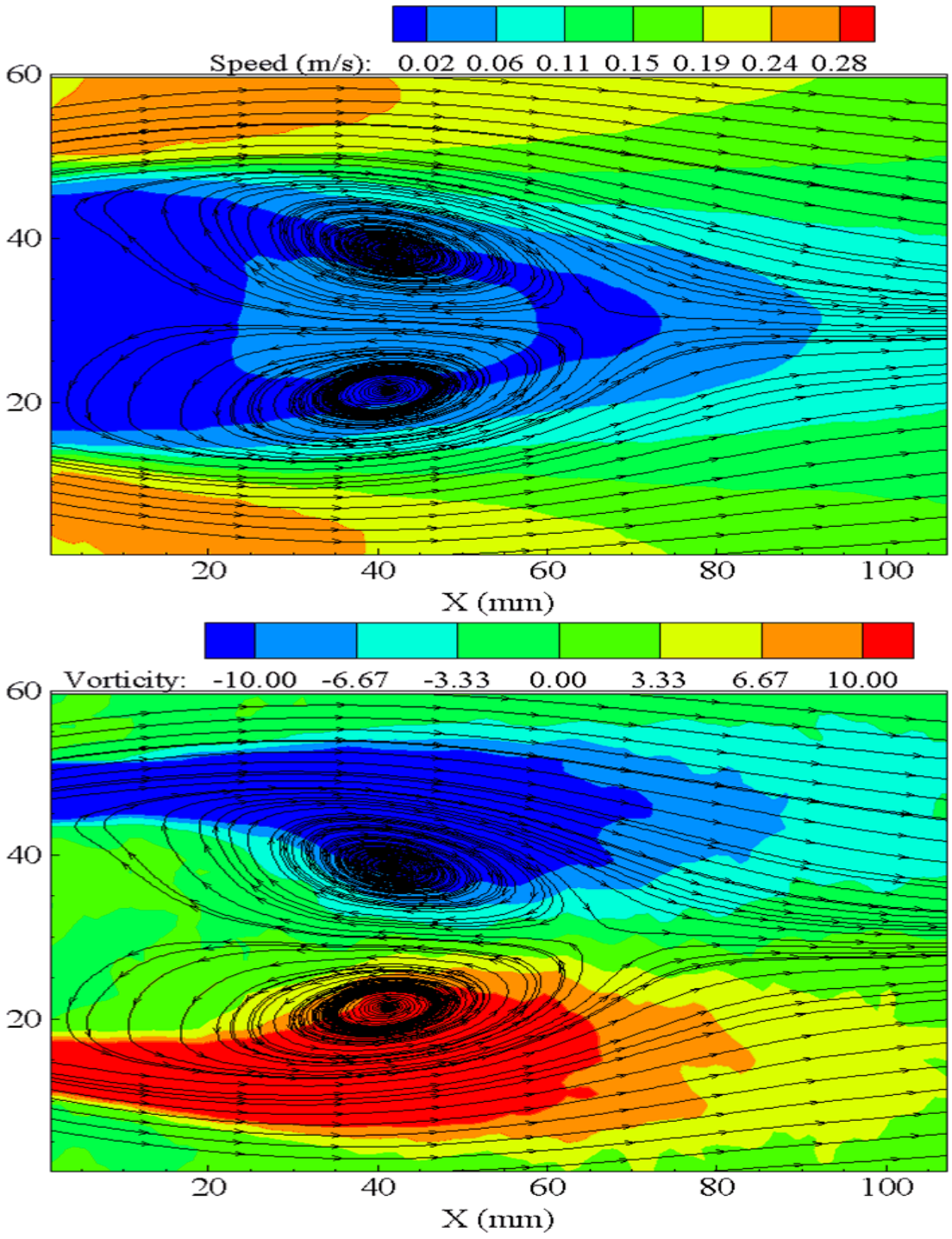

Figure 7-6: Flow field and vorticity plot at a downstream of bluff body

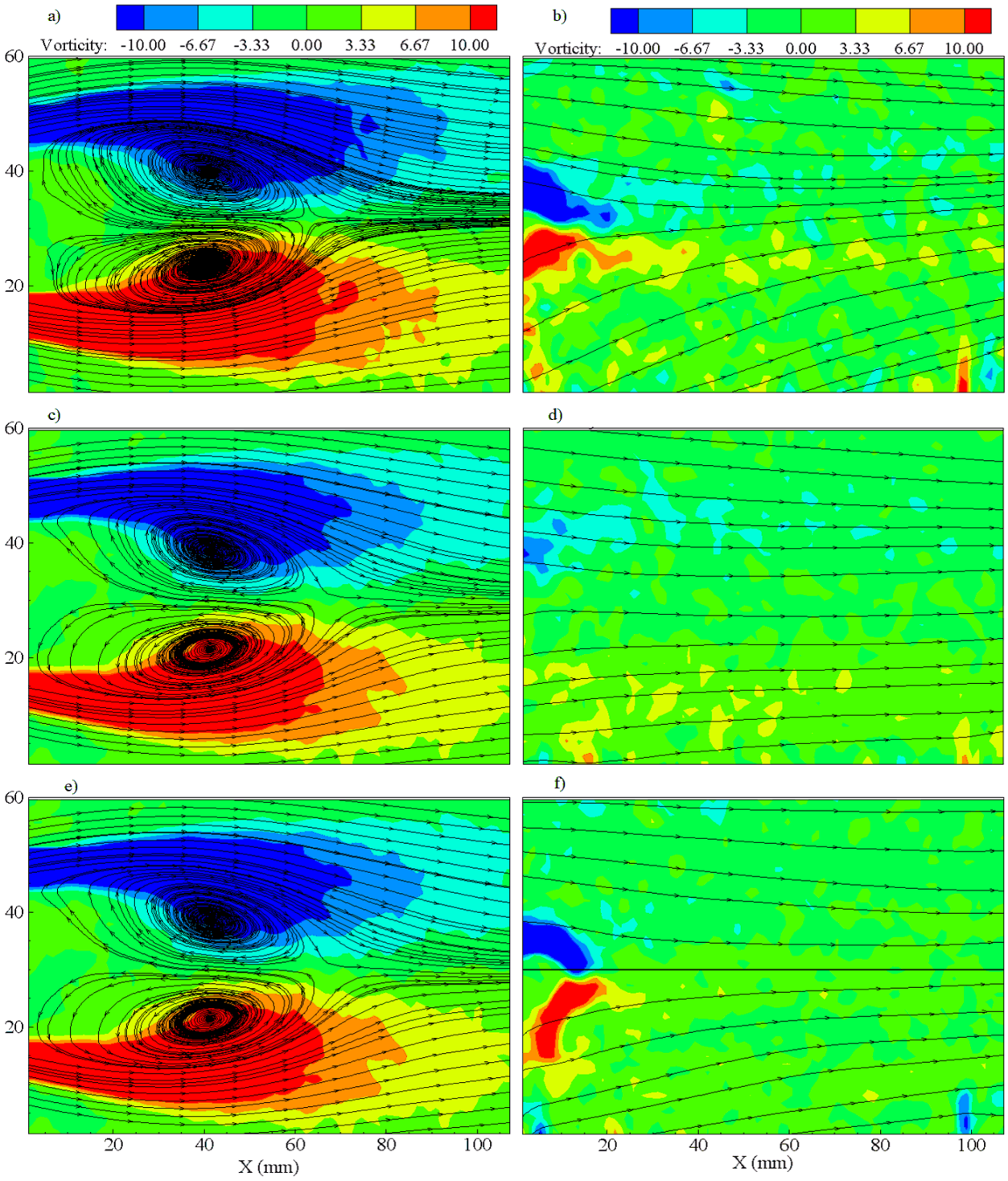

Figure 7-7: Vorticity surface plot of maximum flapping envelope at $\gamma = 0.001N.m, \gamma = 0.0015N.m$ *and* $\gamma = 0.002N.m$ a) vorticity surface plot at $\gamma = 0.001N.m$ after flow past a circular cylinder b)vorticity at $\gamma = 0.001N.m$ after trailing edge of an inverted flag c) vorticity at $\gamma = 0.0015N.m$ after a circular cylinder d)vorticity plot at $\gamma = 0.0015N.m$ after trailing edge e)vorticity at $\gamma = 0.002N.m$ after a circular cylinder f) vorticity plot at $\gamma = 0.002N.m$ after trailing edge of an inverted piezoelectric flag.

REFERENCES

[1] S. Michelin and D. Doaré, “Energy harvesting efficiency of piezoelectric flags in axial flows,” *J. Fluid Mech.*, vol. 714, pp. 489–504, 2013.

[2] D. Kim, J. Cossé, C. Huertas Cerdeira, and M. Gharib, “Flapping dynamics of an inverted flag,” *J. Fluid Mech.*, vol. 736, pp. 1–12, 2013.

[3] J. Ryu, S. G. Park, B. Kim, and H. J. Sung, “Flapping dynamics of an inverted flag in a uniform flow,” *J. Fluids Struct.*, vol. 57, pp. 159–169, 2015.

[4] J. E. Sader, J. Cossé, D. Kim, B. Fan, and M. Gharib, “Large-amplitude flapping of an inverted flag in a uniform steady flow-a vortex-induced vibration,” *J. Fluid Mech.*, vol. 793, no. December, pp. 524–555, 2016.

[5] E. Uddin, W. X. Huang, and H. J. Sung, “Actively flapping tandem flexible flags in a viscous flow,” *J. Fluid Mech.*, vol. 780, no. August, pp. 120–142, 2015.

[6] S. Alben and M. J. Shelley, “Flapping states of a flag in an inviscid fluid: Bistability and the transition to chaos,” *Fluid Dyn. Res.*, vol. 46, no. 5, pp. 3–6, 2014.

[7] M. Argentina and L. Mahadevan, “Fluid-flow-induced flutter of a flag,” *Proc. Natl. Acad. Sci. U. S. A.*, vol. 102, no. 6, pp. 1829–1834, 2005.

[8] S. Michelin, S. G. L. Smith, and B. J. Glover, “Vortex shedding model of a flapping flag,” *J. Fluid Mech.*, vol. 617, pp. 1–10, 2008.

[9] C. Eloy, C. Souilliez, and L. Schouveiler, “Flutter of a rectangular cantilevered plate,” *Am. Soc. Mech. Eng. Press. Vessel. Pip. Div. PVP*, vol. 9, no. December 2006, pp. 407–416, 2006.

[10] B. S. H. Connell and D. K. P. Yue, *Flapping dynamics of a flag in a uniform stream*, vol. 581. 2007.

[11] E. Uddin, W. X. Huang, and H. J. Sung, “Interaction modes of multiple flexible flags in a uniform flow,” *J. Fluid Mech.*, vol. 729, pp. 563–583, 2013.

[12] C. B. Sun, S. Y. Wang, L. B. Jia, and X. Z. Yin, “Force measurement on coupled flapping flags in uniform flow,” *J. Fluids Struct.*, vol. 61, pp. 339–346, 2016.

[13] C. P. Shao, Y. J. Chen, and J. Z. Lin, “Wind induced deformation and vibration of a Platanus acerifolia leaf,” *Acta Mech. Sin. Xuebao*, vol. 28, no. 3, pp. 583–594, 2012.

[14] S. Orrego *et al.*, “Harvesting ambient wind energy with an inverted piezoelectric flag,” *Appl. Energy*, vol. 194, pp. 212–222, 2017.

[15] J. Sader and D. Kim, “Pvp2014-28445 the Effect of Aspect Ratio and Angle of Attack on the Transition,” pp. 2–6, 2014.

[16] S. Rinaldi and M. P. Païdoussis, “Theory and experiments on the dynamics of a free-clamped cylinder in confined axial air-flow,” *J. Fluids Struct.*, vol. 28, pp. 167–179, 2012.

[17] C. Tang, N. S. Liu, and X. Y. Lu, “Dynamics of an inverted flexible plate in a uniform flow,” *Phys. Fluids*, vol. 27, no. 7, 2015.

[18] K. Shoele and R. Mittal, “Energy harvesting by flow-induced flutter in a simple model of an

inverted piezoelectric flag," *J. Fluid Mech.*, vol. 790, pp. 582–606, 2016.

[19] H. Kim, S. Kang, and D. Kim, "Dynamics of a flag behind a bluff body," *J. Fluids Struct.*, vol. 71, pp. 1–14, 2017.

[20] M. M. B. Tofa, A. Maimun, and Y. M. Ahmed, "Fundamentals of vortex induced vibration analysis of marine riser," no. September, 2012.

[21] M. Nishioka and H. Sato, "Mechanism of determination of the shedding frequency of vortices behind a cylinder at low Reynolds numbers," *J. Fluid Mech.*, vol. 89, no. 1, pp. 49–60, 1978.

[22] A. Maas, "Local and global gauge-fixing," *Proc. Sci.*, pp. 473–537, 2012.

[23] M. Gaster, "Vortex shedding from circular cylinders at low Reynolds numbers," *J. Fluid Mech.*, vol. 46, no. 4, pp. 749–756, 1971.

[24] J. H. Lienhard, "Synopsis of lift, drag, and vortex frequency data for rigid circular cylinders," *Bulletin 300*. pp. 1–36, 1966.

[25] C. K. Choi and D. K. Kwon, "Wind tunnel blockage effects on aerodynamic behavior of bluff body," *Wind Struct. An Int. J.*, vol. 1, no. 4, pp. 351–364, 1998.

[26] S. Annapureddy, S. Acharya, A. Gilmanov, and H. Stolarski, "Experimental and numerical investigation of the oscillation of an inverted flag," *10th Int. Symp. Turbul. Shear Flow Phenomena, TSFP 2017*, vol. 1, no. 2012, 2017.

[27] J. Silva-Leon, A. Cioncolini, M. R. A. Nabawy, A. Revell, and A. Kennaugh, "Simultaneous wind and solar energy harvesting with inverted flags," *Appl. Energy*, vol. 239, no. January, pp. 846–858, 2019.